JPL Publication 87-8

(MSAT-X Report No. 144)

The Performance of Trellis Coded Multilevel DPSK on a Fading Mobile Satellite Channel

Marvin K. Simon
Dariush Divsalar

June 1, 1987

National Aeronautics and
Space Administration

Jet Propulsion Laboratory
California Institute of Technology
Pasadena, California

JPL Publication 87-8 (MSAT-X Report No. 144)

The Performance of Trellis Coded Multilevel DPSK on a Fading Mobile Satellite Channel

Marvin K. Simon
Dariush Divsalar

June 1, 1987

National Aeronautics and
Space Administration

Jet Propulsion Laboratory
California Institute of Technology
Pasadena, California

The research described in this publication was carried out by the Jet Propulsion Laboratory, California Institute of Technology, under a contract with the National Aeronautics and Space Administration.

Abstract

In this report, we consider the performance of trellis coded multilevel differential phase-shift-keying (MDPSK) over Rician and Rayleigh fading channels. For operation at L-Band, this signaling technique leads to a more robust system than the coherent system with dual pilot tone calibration previously proposed for UHF. The results are obtained using a combination of analysis and simulation. The analysis shows that the design criterion for trellis codes to be operated on fading channels with interleaving/deinterleaving is no longer free Euclidean distance. The correct design criterion for optimizing bit error probability of trellis coded MDPSK over fading channels will be presented along with examples illustrating its application.

CONTENTS

Figures

Figures

I. Introduction

In a previous report [1], the authors considered the performance of trellis coded multilevel phase-shift-keying (MPSK) when transmitted over a fading mobile satellite channel. Such a channel is characterized by Rician fading which can be described by a single parameter K corresponding to the ratio of power in the total coherent (direct plus specular) component to that in the noncoherent (diffuse) component. The analysis was carried out under the assumption of ideal coherent detection, i.e., the effect of the fading on the phase of the received signal was fully compensated for at the receiver. Thus, the numerical results derived from this analysis reflected only the degradation due to the effect of the fading on the amplitude of the received signal.

Although most of the discussion and numerical results presented in [1] pertained to this idealistic assumption, mention was made of the fact that, in an actual implementation, the carrier demodulation function would typically be performed using pilot tone calibration techniques [2, 3]. Assuming a dual tone calibration technique [4] wherein two tones of equal power are inserted symmetrically at the edges of the data spectrum for the purpose of deriving a coherent demodulation reference, simulation results presented in [1] showed that the noisy carrier reference so produced resulted in a signal-to-noise ratio degradation of about 2 to 3 dB depending on the value of the Rician parameter K. This rather large degradation is caused by the fact that the bandwidth of the pilot tone bandpass filters has to be chosen wide enough to accommodate the maximum doppler (on the order of 100 Hz at UHF for a land mobile vehicle travelling at 80 mph) and that some of the total transmitted power has to be allocated to the two pilot tones thus robbing the data-bearing signal.

Under these circumstances, it is reasonable to consider the performance of trellis coded multilevel differential phase-shift-keying (MDPSK) with the hope that the performance penalty associated with the differential detector will not exceed that due to the noisy carrier demodulation reference in the coherent system. If this is indeed true (as we will be shown in this report), then the MDPSK system has a decided implementation advantage over the coherent MPSK one in that a means for extracting a carrier demodulation reference does not have to be provided. The results will be obtained using a combination of analysis and simulation. Also, as in [1] we shall consider only the case where interleaving/deinterleaving is employed to combat the fading. This allows for considerable simplification of the analysis and is of great practical interest.

II. System Model

Figure 1 is a simplified block diagram of the system under investigation. Input bits representing data or digitally encoded speech and occurring at a rate R_b are passed through a rate $n/(n + 1)$ trellis encoder producing an encoded symbol stream at a rate $[(n + 1)/n]R_b$. The encoder output symbols are then block interleaved to break up burst errors caused by amplitude fades of duration greater than one symbol time.

While in practice the depth of interleaving is finite and chosen in relation to the maximum fade duration anticipated which in turn is related to the maximum doppler frequency produced by the mobile's movement, we shall make the usual assumption of infinite interleaving depth. Our simulation results will, however, reflect a finite interleaving depth necessitated by practical limitations on the total coding/decoding delay in a speech transmission system

[1]. Thus, these results will be slightly pessimistic when compared with those derived from theory. The primary purpose of the analysis is to indicate through simple example the trend of the performance behavior as a function of the various system parameters leaving the actual numerical performance to be predicted by the software simulations.

The interleaved trellis-encoded symbols are next mapped, in groups of $n + 1$, into an $M = 2^n + 1$ - level PSK signal set according to the set partitioning method [5]. The MPSK symbols are then differentially encoded and modulated onto an RF carrier for transmission over the channel. Since the MDPSK symbol rate is R_b/n, it is reasonable, from a conservation of bandwidth standpoint, to compare the performance of this system to an uncoded $M = 2^n$ - level DPSK system with the identical input bit rate.

At the receiver, the faded, noise-corrupted signal is differentially detected and the resulting symbols are then deinterleaved. The trellis decoder is implemented as a Viterbi algorithm with a metric depending upon whether or not channel state information (CSI) is provided [6]. A measure of CSI can be obtained from envelope detection of the received signal.

In selecting a decoding metric, a tradeoff exists between simplicity of implementation and the optimality associated with the degree to which the metric matches the differential detector output statistics. For the case of uncoded MDPSK, a metric based on minimizing the distance between the received and transmitted signal vectors (equivalent to assuming Gaussian statistics as in the coherent MPSK analysis of [1]) is optimum in the sense of a minimum probability of error test. For the coded case, the optimum (maximum-likelihood) metric would depend on the joint two-dimensional (amplitude and phase) statistics of a sequence of receptions.

In this report, we shall consider both the maximum-likelihood (truly matched) and the much simpler to implement (and analyze) Gaussian metric. System performance results for the latter will be obtained through a combination of analysis and simulation.

III. Analysis Model

The basic analysis model for the block diagram of Figure 1 is illustrated in Figure 2. The box labelled encoder is actually the combination of the trellis encoder and the mapping function of Figure 1. We denote a coded symbol sequence of length N by

$$\underline{x} = (x_1, x_2, \ldots, x_N) \tag{1}$$

where the kth element of $\underline{x}$, namely x_k, represents the transmitted MPSK symbol in the kth transmission interval and, in general, is a nonlinear function of the state of the encoder s_k and the n information bits $\underline{u}$, at its input. Before transmission over the channel, the sequence $\underline{x}$ is differentially encoded producing the sequence $\underline{v}$. In phasor notation, v_k and v_{k+1} can be written as

$$v_k = \sqrt{2E_s}\, e^{j\phi_k}$$

$$v_{k+1} = v_k\, x_{k+1} = \sqrt{2E_s}\, e^{j(\phi_k+\Delta\phi_{k+1})} = \sqrt{2E_s}\, e^{j\phi_{k+1}} \tag{2}$$

where $E_s = nE_b$ is the energy per MDPSK symbol and

$$x_k = e^{j\Delta\phi_k} \tag{3}$$

is the phasor representation of the MPSK symbol $\Delta\phi_k$ assigned by the mapper in the kth transmission interval.

Corresponding to $\underline{x}$, the channel outputs the sequence

$$\underline{y} = (y_1, y_2, \ldots, y_N) \tag{4}$$

where the k + 1st element y_{k+1}, representing the output in the k + 1st transmission interval, is given by

$$\begin{aligned} y_{k+1} &= w_k^* w_{k+1} \\ &= \left(X_k^* \sqrt{2E_s}\, e^{-j\phi_k} + N_k^* \right) \left(X_{k+1} \sqrt{2E_s}\, e^{j(\phi_k + \Delta\phi_{k+1})} + N_{k+1} \right) \\ &= X_k^* X_{k+1}\, 2E_s\, e^{j\Delta\phi_{k+1}} + \text{noise terms} \end{aligned} \tag{5}$$

Here N_k, N_{k+1} are samples of a stationary, complex Gaussian noise process N(t) which represents the additive thermal noise at the receiver front end, and X_k, X_{k+1} are samples of a normalized, stationary, complex Gaussian noise process X(t) (independent of N(t)) which represents the fading characteristic of the mobile satellite channel. The first two moments of the random variables (r.v.'s) X_k and N_k are given by

$$E\{X_k\} = \mu \; ; \; E\{|X_k|^2\} - |\mu|^2 = \sigma^2 \; ; \; \sigma^2 + |\mu|^2 = 1$$

$$E\{N_k\} = 0 \; ; \; E\{N_k N_\ell^*\} = 2N_0 \delta_{k\ell} \tag{6}$$

Writing X_k in the phasor form

$$X_k = \rho_k\, e^{j\phi_k} \tag{7}$$

we see that ρ_k is a normalized (unit mean-squared value) r.v. with a Rician probability density function (p.d.f.) given by

$$p(\rho_k) = \begin{cases} 2\rho_k(1 + K) \exp[-K - \rho_k^2(1 + K)]\, I_0(2\rho_k \sqrt{K(1 + K)}); \; \rho_k \geq 0 \\ 0 \; ; \text{ otherwise} \end{cases} \tag{8}$$

where once again the parameter K represents the ratio of powers of the coherent to noncoherent fading components. Finally, if CSI is available, then the corresponding side information sequence $\underline{z}$ will be denoted by

$$\underline{z} = (z_1, z_2, \ldots, z_N) \tag{9}$$

As previously stated, we shall assume infinite depth interleaving and deinterleaving so that the coding channel is memoryless. Under this assumption, the products $\rho_k \rho_{k+1}$ are independent r.v.'s and hence the joint channel probabilities satisfy

$$p_N(\underline{y}|\underline{x},\underline{z}) = \prod_{n=1}^{N} p(y_n|x_n,z_n) \tag{10a}$$

and

$$q_N(\underline{z}) = \prod_{n=1}^{N} q(z_n) \tag{10b}$$

IV. The Maximum-Likelihood Metric for Coded MDPSK

For any coded communication system, the decoding process uses a metric of the form $m(\underline{y},\underline{x};\underline{z})$ if side information is available and $m(\underline{y},\underline{x})$ if it is not. Whatever metric is selected, it is desirable from the standpoint of simplifying the decoding process that it have an additive property, namely that the total metric for a sequence of symbols is the sum of the metrics for each channel input and output pair, i.e.,

$$m(\underline{y},\underline{x},\underline{z}) = \sum_{n=1}^{N} m(y_n,x_n;z_n) \tag{11}$$

The maximum-likelihood metric

$$m(\underline{y},\underline{x};\underline{z}) = \log p_N(\underline{y}|\underline{x},\underline{z}) \tag{12a}$$

when side information is available or

$$m(\underline{y},\underline{x}) = \log p_N(\underline{y}|\underline{x}) \tag{12b}$$

when no side information is available satisfies the requirement in (11). This is easily seen by substituting (10) in (11) and recalling that the logarithm of a product equals the sum of the logarithms. Thus, to evaluate (11) we need to obtain the marginal p.d.f. $p(y_n|x_n,z_n)$, take its logarithm, and sum the results.

Assuming perfect side information, i.e., $z_n = \rho_n$, the characteristic function method is used in Appendix A to derive $p(y_n|x_n,z_n)$ with the result

$$p(y_n|x_n,z_n) = \int_0^\infty \frac{R}{2\pi(1 + N_0^2R^2)} \exp\left\{ - \frac{2\rho_n^2 E_s N_0 R^2}{1 + N_0^2R^2} \right\} \times J_0\left(R \left| y_n - \frac{2\rho_n^2 E_s x_n}{1 + N_0^2R^2} \right| \right) dR \tag{13}$$

where $J_0(x)$ is the zero order Bessel function of the first kind. The logarithm of (13) gives the maximum-likelihood branch metric $m(y_n|x_n,z_n)$ which is quite complicated to implement. Furthermore, theoretical analysis of the bit error probability performance of the system in Figure 1 with such a metric is difficult if not impossible.

For this reason, we turn our attention now to the much simpler Gaussian metric for which upper bounds on bit error performance can be readily computed. This approach is analogous to that taken in [7].

V. Derivation of the Pair-Wise Error Probability Bound

To find an upper bound on the average bit error probability performance of the system, we must first find the pair-wise error probability $P(\underline{x} \rightarrow \hat{\underline{x}})$ which represents the probability of choosing the coded sequence $\hat{\underline{x}} = (\hat{x}_1, \hat{x}_2, \ldots, \hat{x}_N)$ instead of $\underline{x} = (x_1, x_2, \ldots, x_N)$. Letting $m(\underline{y},\underline{x};\underline{z})$ denote the coding decision metric, i.e., $\hat{\underline{x}}$ is incorrectly chosen as the transmitted sequence when $m(\underline{y},\hat{\underline{x}};\underline{z}) > m(\underline{y},\underline{x};\underline{z})$, then the pair-wise error probability has the Chernoff bound [6]

$$P(\underline{x} \rightarrow \hat{\underline{x}}) \leq E\{\exp(\lambda[m(\underline{y},\hat{\underline{x}}|\underline{z}) - m(\underline{y},\underline{x}|\underline{z})])|\underline{x}\}$$

$$= \prod_{n\varepsilon\eta} E\{\exp(\lambda[m(y_n,\hat{x}_n|z_n) - m(y_n,x_n|z_n)]|\underline{x}\} \tag{14}$$

where the "E" operator denotes statistical expectation, λ is the Chernoff parameter to be optimized, and η is the set of all n such that $x_n \neq \hat{x}_n$. To simplify (4) any further, we must specify a particular metric and whether or not channel state information is available. As previously stated, we shall use the metric which is optimum (maximum-likelihood) for the additive Gaussian noise channel. We begin by treating the case where CSI is absent.

A. No Channel State Information

When no CSI is provided the Gaussian metric takes the form

$$m(y_n,x_n) = -|y_n - 2E_s x_n|^2 \tag{15}$$

Substituting (5) into (15) and noting from (3) that $|x_n|^2 = |\hat{x}_n|^2 = 1$ independent of n, the difference of the metrics required in (14) becomes

$$m(y_n,\hat{x}_n) - m(y_n,x_n) = -|w_{n-1}^{*}w_n - 2E_s\hat{x}_n|^2 + |w_{n-1}^{*}w_n - 2E_s x_n|^2$$

$$= 2E_s[w_{n-1}^{*}w_n(\hat{x}_n - x_n^{*}) + w_{n-1}w_n^{*}(\hat{x}_n - x_n)] \tag{16}$$

which can be conveniently written in the matrix form

$$m(y_n,\hat{x}_n) - m(y_n,x_n) = 2E_s\underline{W}_n^{*T}(\hat{\underline{A}}_n - \underline{A}_n)\underline{W}_n \tag{17}$$

where

$$\underline{W}_n = \begin{bmatrix} w_{n-1} \\ w_n \end{bmatrix}; \quad \hat{\underline{A}}_n = \begin{bmatrix} 0 & \hat{x}_n^{*} \\ \hat{x}_n & 0 \end{bmatrix}; \quad \underline{A}_n = \begin{bmatrix} 0 & x_n^{*} \\ x_n & 0 \end{bmatrix} \tag{18}$$

and "T" denotes the transpose operation.

From (5) and (7) we have

$$w_{n-1}^{*}w_n = \rho_{n-1}\rho_n\, 2E_s e^{j\Delta\phi_n} + \text{noise terms} \tag{19}$$

Assuming that the fading is slow-varying enough that $\rho_{n-1} = \rho_n$, substituting (17) into (14) gives

$$P(x \to \hat{\underline{x}}) = \overline{P(\underline{x} \to \hat{\underline{x}}|\underline{\rho})}^{\rho};$$

$$P(\underline{x} \to \hat{\underline{x}}|\underline{\rho}) \le \prod_{n\varepsilon\eta} E\left\{\exp\left(\lambda' \underline{W}_n^{*T}(\hat{\underline{A}}_n - \underline{A}_n)\underline{W}_n\right)\Big|x_n,\rho_n\right\} \tag{20}$$

where the expectation is now only over the additive noise, the overbar denotes statistical averaging over the fading, and $\lambda' = 2E_s\lambda$.

The expectation required in (20) was originally evaluated by Stein [8] and later by Johnston [7] in connection with the analysis of a block coded MDPSK system. In particular, for any $n\varepsilon\eta$,

$$E\left\{\exp(\lambda' \underline{W}_n^{*T}(\hat{\underline{A}}_n - \underline{A}_n)\underline{W}_n) | x_n, \rho_n\right\} = \frac{\exp\left\{-\lambda' \underline{\mu}_n^{*T}(\underline{F}_n^{-1} + 2\lambda' \underline{R}_n^{*})^{-1} \underline{\mu}_n\right\}}{\det(\underline{I} + 2\lambda' \underline{R}_n^{*} \underline{F}_n)}$$

$$= \frac{\exp\left\{-\lambda' \underline{\mu}_n^{*T} \underline{F}_n(\underline{I} + 2\lambda' \underline{R}_n^{*} \underline{F}_n)^{-1} \underline{\mu}_n\right\}}{\det(\underline{I} + 2\lambda' \underline{R}_n^{*} \underline{F}_n)} \qquad (21)$$

where $\underline{I}$ is the identity matrix and

$$\underline{F}_n \triangleq \hat{\underline{A}}_n - \underline{A}_n = \begin{bmatrix} 0 & (\hat{x}_n - x_n)^* \\ \hat{x}_n - x_n & 0 \end{bmatrix}$$

$$\underline{\mu}_n = E\{\underline{W}_n | x_n, \rho_n\} = \begin{bmatrix} E\{w_{n-1} | x_n, \rho_n\} \\ E\{w_n | x_n, \rho_n\} \end{bmatrix} \triangleq \begin{bmatrix} \mu_{n-1} \\ \mu_n \end{bmatrix}$$

$$\underline{R}_n = \frac{1}{2} E\{(\underline{W}_n - \underline{\mu}_n)^*(\underline{W}_n - \underline{\mu}_n)^T | x_n, \rho_n\}$$

$$= \frac{1}{2} \begin{bmatrix} E\{|w_{n-1} - \mu_{n-1}|^2\} & E\{(w_{n-1} - \mu_{n-1})^*(w_n - \mu_n)\} \\ E\{(w_{n-1} - \mu_{n-1})(w_n - \mu_n)^*\} & E\{|w_n - \mu_n|^2\} \end{bmatrix} \qquad (22)$$

Also, it should be noted that (17) is valid only when $\det(\underline{I} + 2\lambda' \underline{R}_n^{*} \underline{F}_n) > 0$.

After much manipulation, (21) evaluates to

$$E\{\exp(\lambda' \underline{W}_n^{*T}(\hat{\underline{A}}_n - \underline{A}_n)\underline{W}_n) | x_n, \rho_n\} =$$

$$\frac{\exp\left\{4\lambda_0 \frac{E_s}{N_0} \rho_n^2 \left[\frac{2\lambda_0 |\hat{x}_n - x_n|^2 + \mathrm{Re}\{x_n(\hat{x}_n - x_n)^*\}}{1 - (2\lambda_0)^2 |\hat{x}_n - x_n|^2}\right]\right\}}{1 - (2\lambda_0)^2 |\hat{x}_n - x_n|^2} \tag{23}$$

where $\lambda_0 = \lambda' N_0 = 2E_s N_0 \lambda$.

One further simplification of (23) is possible for constant envelope signal sets such as MDPSK. In particular, it can easily be shown that

$$|\hat{x}_n - x_n|^2 = -2\mathrm{Re}\{x_n(\hat{x}_n - x_n)^*\} \tag{24}$$

Substituting (24) into (23) and then into (20) gives the desired result for the conditional (on ρ_n) pair-wise error probability bound, namely,

$$P(\underline{x} \to \hat{\underline{x}} | \underline{\rho}) \leq \prod_{n \varepsilon \eta} \frac{\exp\left\{\frac{2\lambda_0 \frac{E_s}{N_0} \rho_n^2 |\hat{x}_n - x_n|^2 (1 - 4\lambda_0)}{1 - (2\lambda_0)^2 |\hat{x}_n - x_n|^2}\right\}}{1 - (2\lambda_0)^2 |\hat{x}_n - x_n|^2} \tag{25}$$

It remains to average (25) over the p.d.f. of ρ_n given in (8) and then optimize over the Chernoff parameter.

Since we have assumed that the fading is constant over two symbol intervals, i.e., $\rho_{n-1}\rho_n$ has been replaced by ρ_n^2, and that the interleaving/deinterleaving makes the ρ_n's independent, then the average over $\underline{\rho}$ in (20) can, insofar as the upper bound is concerned, be computed as the product of the averages. Averaging each term in the product of (25) over the p.d.f. in (8) gives*

*For simplicity of notation, we herein drop the zero subscript on λ.

$$\frac{\exp\left\{-\dfrac{2\lambda \dfrac{E_s}{N_0}\rho_n^2 |\hat{x}_n - x_n|^2(1-4\lambda)}{1-(2\lambda)^2|\hat{x}_n - x_n|^2}\right\}}{1-(2\lambda)^2|\hat{x}_n - x_n|^2}^{\rho_n} =$$

$$\frac{1+K}{1+K+|\hat{x}_n - x_n|^2\left[2\lambda \dfrac{\bar{E}_s}{N_0}(1-4\lambda) - (2\lambda)^2(1+K)\right]}$$

$$\times \exp\left\{-K \frac{2\lambda \dfrac{\bar{E}_s}{N_0}(1-4\lambda)|\hat{x}_n - x_n|^2}{1+K+|\hat{x}_n - x_n|^2\left[2\lambda \dfrac{\bar{E}_s}{N_0}(1-4\lambda) - (2\lambda)^2(1+K)\right]}\right\} \quad (26)$$

For the Rayleigh case (K = 0), (26) simplifies to

$$\frac{\exp\left\{-\dfrac{2\lambda \dfrac{E_s}{N_0}\rho_n^2 |\hat{x}_n - x_n|^2(1-4\lambda)}{1-(2\lambda)^2|\hat{x}_n - x_n|^2}\right\}}{1-(2\lambda)^2|\hat{x}_n - x_n|^2}^{\rho_n} =$$

$$\frac{1}{1+|\hat{x}_n - x_n|^2\left[2\lambda \dfrac{\bar{E}_s}{N_0}(1-4\lambda) - (2\lambda)^2\right]} \quad (27)$$

The result in (26) cannot be optimized over λ independent of the index n. Thus, for the Rician case, we first must compute the pair-wise error probability (or better yet, the average bit error probability) and then optimize over the Chernoff parameter. On the other hand, the result in (27) can be optimized over λ independent of n. In particular, we wish to choose λ to maximize the term in brackets in the denominator of (27).

Differentiating this expression with respect to λ and equating the result to zero give the optimum Chernoff parameter

$$\lambda_{opt} = \frac{\bar{E}_s/4N_0}{1 + 2\bar{E}_s/N_0} \tag{28}$$

Substituting (28) in (27) and simplifying give the upper bound on pair-wise error probability for the Rayleigh channel:

$$P(\underline{x} \to \hat{\underline{x}}) \leq \prod_{n \in \eta} \frac{1 - \nu^2}{1 - \nu^2\left(1 - \left|\frac{\hat{x}_n - x_n}{2}\right|^2\right)} \tag{29}$$

where

$$\nu = \frac{\bar{E}_s/N_0}{1 + \bar{E}_s/N_0} \tag{30}$$

1. Derivation of the Bit Error Probability Bound

An upper bound on the average bit error probability is obtained from the pair-wise error probability bound as

$$P_b \leq \sum_{\underline{x},\hat{\underline{x}}} \sum_{\varepsilon \mathscr{C}} a(\underline{x},\hat{\underline{x}}) p(\underline{x}) P(\underline{x} \to \hat{\underline{x}}) \tag{31}$$

where $a(\underline{x},\hat{\underline{x}})$ is the number of bit errors that occur when $\underline{x}$ is transmitted and $\hat{\underline{x}}$ is chosen by the decoder, $p(\underline{x})$ is the a priori probability of transmitting $\underline{x}$ and $\mathscr{C}$ is the set of all coded sequences. An efficient procedure for evaluating (31) is the transfer function bound approach taken in [9]. In particular, the trellis code is represented by a pair-state transition diagram [10]. Each pair-state $(s_k,\hat{s}_k)$ corresponds to a pair of states s_k and $\hat{s}_k$ in the trellis diagram. Thus, a transition between pair states $(s_k,\hat{s}_k)$ and

$(s_{k+1}, \hat{s}_{k+1})$ in the transition diagram corresponds to a pair of transitions in the trellis diagram, i.e., s_k to s_{k+1} and $\hat{s}_k$ to $\hat{s}_{k+1}$. Associated with each of these trellis diagram transitions are an MPSK symbol being outputted by the mapper and a corresponding sequence of n input bits (an information symbol) to the encoder. Thus, the transition between two pair-states in the transition diagram is characterized by the squared Euclidean distance δ^2 between the corresponding MPSK output symbols and the Hamming distance Ω between the corresponding input bit sequences.

Based on the above discussion, in the absence of fading, each branch between pair states in the transition diagram has a gain G of the form

$$G = \sum \frac{1}{2^n} I^{\Omega} D^{\delta^2} \tag{32}$$

Here I is an index, D is the Bhattacharyya distance defined by

$$D = \exp\left(-\frac{nE_b}{4N_0}\right) \tag{33}$$

and the summation accounts for the possibility of parallel paths between states in the trellis diagram. The transfer function (the sum of all possible path gains) of the transition diagram is denoted by T(D,I) and, by comparison with (31), the upper bound on average bit error probability is given by

$$P_b \leq \frac{1}{n} \frac{d}{dI} T(D,I)\Big|_{I=1} \tag{34}$$

Since, for no fading, the factor D^{δ^2} in (32) is analogous to the corresponding term in the product describing $P(\underline{x} \rightarrow \hat{\underline{x}})$, for the fading case we make the same association. In particular, for a given branch label gain, D^{δ^2} would be

replaced by (26) or (27) as appropriate with $|\hat{x}_n - x_n|^2$ representing the Euclidean distance between pair-states as discussed above.

2. An Example

Consider the case of rate 1/2 trellis coded asymmetric QPSK using a simple 2-state trellis. The appropriate set partitioning is illustrated in Figure 3, the trellis diagram in Figure 4, and pair-state transition diagram in Figure 5. The performance of this system in the absence of fading and with coherent detection was treated in [9] with the following results:

$$T(D,I) = \frac{4ac}{1 - 2b};\ a = \frac{I}{2}D^4;\ b = \frac{I}{2}D^{\frac{4}{1+\alpha}};\ c = \frac{1}{2}D^{\frac{4\alpha}{1+\alpha}} \tag{35}$$

Here α is the ratio of powers between the I and Q channels which is related to the angle ϕ that defines the asymmetry (see Figure 3) by

$$\alpha = \tan^2 \frac{\phi}{2} \tag{36}$$

Also, note the branch gains a, b, and c are of the form in (32). Substituting (35) into (34) gives

$$P_b \leq \frac{D^{\frac{4(1+2\alpha)}{1+\alpha}}}{\left(1 - D^{\frac{4}{1+\alpha}}\right)^2} \tag{37}$$

which when optimized over the asymmetry produces the desired upper bound

$$P_b \leq \frac{27}{4} \exp(-2E_b/N_0) \tag{38}$$

Based upon the above discussion, for differential detection in the presence of Rayleigh fading, the transfer function of (35) applies with, however, a, b, and c defined by

$$a = \frac{I}{2}(1 - \upsilon^2)$$

$$b = \frac{I}{2}\,\frac{1 - \upsilon^2}{1 - \upsilon^2\left(\frac{\alpha}{1+\alpha}\right)}$$

$$c = \frac{1}{2}\,\frac{1 - \upsilon^2}{1 - \upsilon^2\left(\frac{1}{1+\alpha}\right)} \tag{39}$$

Performing the differentiation required in (34) gives upon simplification

$$P_b \leq \left(\frac{1-\upsilon^2}{\upsilon^2}\right)^2 \frac{\left(1 + \alpha - \upsilon^2\alpha\right)^2(1+\alpha)}{1 + \alpha - \upsilon^2} \tag{40}$$

For a symmetric QPSK signal set ($\alpha = 1$), (40) reduces to

$$P_b \leq 2\left(\frac{1 - \upsilon^2}{\upsilon^2}\right)^2 (2 - \upsilon^2) \tag{41}$$

On the other hand, optimizing (40) with respect to α produces the optimum asymmetry condition

$$\alpha_{opt} = -\left(1 - \frac{3\upsilon^2}{4}\right) + \sqrt{\left(1 - \frac{3\upsilon^2}{4}\right)^2 - \left(1 - \upsilon^2 - \frac{\upsilon^2}{2(1-\upsilon^2)}\right)} \tag{42}$$

which can then be substituted into (40) to give the optimized bit error rate performance bound.

Illustrated in Figure 6 is the upper bound on bit error probability performance for the symmetric signal set as given by (41) and the comparable upper bound for the optimized asymmetric signal set as determined from (40) together with (42). Also shown in this figure are the corresponding results for ideal coherent detection as obtained in [1]. Finally, the results for

uncoded BPSK (same bandwidth as rate 1/2 trellis coded QPSK) are superimposed on the same figure. Although the performance of uncoded BPSK over a Rayleigh channel can be obtained in exact closed form, for fairness of comparison, the uncoded performance curves in Figure 6 are upper bounds determined from the same Chernoff bound approach as was used for the coded results. For MPSK, these bounds are mathematically given by

$$P_b \leq \sum_{m=1}^{M-1} \frac{1 - v^2}{1 - v^2 \cos^2 \frac{\pi m}{M}} \tag{43a}$$

for differential detection and

$$P_b \leq \sum_{m=1}^{M-1} \frac{1}{1 + \left(\sin^2 \frac{\pi m}{M}\right)\left(\frac{\bar{E}_s}{N_0}\right)} \tag{44a}$$

for coherent detection. When M=2 (BPSK), these results simplify to

$$P_b \leq 1 - v^2 = \frac{1 + 2\bar{E}_b/N_0}{(1 + \bar{E}_b/N_0)^2} \tag{43b}$$

and

$$P_b \leq \frac{1}{1 + \bar{E}_b/N_0} \tag{44b}$$

We observe from Figure 6 the interesting result that, over the range of $\bar{E}_b/N_0$ considered, the differential detection results track the coherent detection results with a fixed $\bar{E}_b/N_0$ difference of about 1.5 dB for the coded cases and about 3 dB for the uncoded case.

For differential detection in the presence of Rician fading, the transfer function of (35) is again applied with, however, a, b, and c now defined by

$$a = \frac{I}{2}\,\xi_1 D^{\zeta_1}$$

$$b = \frac{I}{2}\,\xi_2 D^{\zeta_2}$$

$$c = \frac{1}{2}\,\xi_3 D^{\zeta_3} \tag{45}$$

where

$$\xi_i = \frac{1 + K}{1 + K + \delta_i^2\left[2\lambda\,\frac{\bar{E}_b}{N_0}(1-4\lambda) - (2\lambda)^2(1+K)\right]}$$

$$\zeta_i = \frac{\delta_i^2 K\,(8\lambda)(1-4\lambda)}{1 + K + \delta_i^2\left[2\lambda\,\frac{\bar{E}_b}{N_0}(1-4\lambda) - (2\lambda)^2(1+K)\right]}\;;\; i = 1,\ 2,\ 3 \tag{46}$$

with

$$\delta_1^2 = 4\;;\; \delta_2^2 = \frac{4}{1+\alpha}\;;\; \delta_3^2 = \frac{4\alpha}{1+\alpha} \tag{47}$$

Once again performing the differentiation required in (34) and recalling that we must now also minimize over the Chernoff parameter λ as well as the asymmetry parameter α, we get the following result:

$$P_b \leq \min_{\lambda \geq 0}\ \min_{\alpha}\ \frac{\xi_1 \xi_3 D^{\zeta_1+\zeta_3}}{\left(1 - \xi_2 D^{\zeta_2}\right)^2} \tag{48}$$

Figure 7 is a plot of (48) versus $\bar{E}_b/N_0$ for a Rician parameter $K = 10$ (typical of the mobile satellite channel). Also shown are the results for the symmetric signal set, i.e., the minimization over α in (48) is not performed; instead $\alpha = 1$ is used. Finally, the upper bound on the performance of uncoded BPSK in the same environment, namely,

$$P_b \leq \min_{\lambda} \xi_1 D^{\zeta_1} \tag{49}$$

is also shown. This result is a special case (M = 2) of the more general result for uncoded MPSK, i.e.,

$$P_b \leq \min_{\lambda} \sum_{m=1}^{M-1} \xi_m D^{\zeta_m} \tag{50}$$

where, rather than (47), $\delta_m^2 \triangleq 4 \sin^2 \pi m/M$; m = 1, 2,..., M is used in (46).

As was done in Figure 6, the comparable results for coherent detection, as obtained from [1], are superimposed on this same figure. We observe that once again, over a large range of $\bar{E}_b/N_0$ values (where the curves are approximately straight lines), the results for differential detection track the coherent detection results with a fixed difference of about 1.5 dB for the coded cases and about 2 dB for the uncoded case.

3. Another Example

As another example, consider a rate 2/3 trellis coded asymmetric 8-PSK modulation again using a simple 2-state trellis. The appropriate set partitioning is illustrated in Figure 8, the trellis diagram in Figure 9, and the pair-state transition diagram in Figure 10. The performance of this system in the absence of fading and with coherent detection was also treated in [9] with the following results:

$$T(D,I) = 2d + \frac{2(a_1 + a_2)\, c}{1 - 2b};$$

$$a_1 = \frac{1}{2}\left[D^{\delta_1^2} I^2 + D^{\delta_5^2} I\right] \qquad c = \frac{1}{2}\left[D^{\delta_6^2}(I + 1)\right]$$

$$a_2 = \frac{1}{2}\left[D^{\delta_1^2} I + D^{\delta_5^2} I^2\right] \qquad d = \frac{1}{2}\left[D^{\delta_4^2} I\right]$$

$$b = \frac{1}{2}\left[D^{\delta_7^2} I + D^{\delta_3^2} I^2\right] \tag{51}$$

The set of squared distances from signal point 0 to signal point j = 1,2,3,...,7, denoted by δj^2, are given by

$$\delta_1^2 = 4 \sin^2 \frac{\phi}{2} = 2\,(1 - \cos\phi); \qquad \delta_5^2 = 4 \sin^2\left(\frac{\pi}{2} - \frac{\phi}{2}\right) = 2\,(1 + \cos\phi)$$

$$\delta_1^2 = 2; \qquad \delta_6^2 = 2$$

$$\delta_3^2 = 4 \sin^2\left(\frac{\pi}{4} + \frac{\phi}{2}\right) = 2\,(1 + \sin\phi); \quad \delta_7^2 = 4 \sin^2\left(\frac{\pi}{4} - \frac{\phi}{2}\right) = 2\,(1 - \sin\phi)$$

$$\delta_4^2 = 4 \tag{52}$$

Applying (34) to (51) gives the upper bound

$$P_b \leq \min_{\phi} \frac{1}{2} D^{\delta_4^2} + \frac{D^{\delta_6^2}\left(D^{\delta_1^2} + D^{\delta_5^2}\right)\left(2 - D^{\delta_7^2}\right)}{\left(1 - D^{\delta_7^2} - D^{\delta_3^2}\right)^2} \tag{53}$$

For differential detection in the presence of Rician fading, the transfer function of (51) still applies with, however, $D^{\delta_i^2}$ replaced by $\xi_i D^{\zeta_i}$; i = 1,2,...,7 where ξ_i and ζ_i are defined in (46) with $\bar{E}_b$ replaced by $\bar{E}_s = 2\bar{E}_b$

but the δ_i^2's are now given by (52). Performing the differentiation required in (34), and recalling that we must now also minimize over the Chernoff parameter λ as well as the asymmetry angle ϕ, we get (53) with the same replacement as above, namely,

$$P_b \leq \min_{\lambda \geq 0} \min_{\phi} \frac{1}{2} \xi_4 D^{\zeta_4} + \frac{\xi_2 D^{\zeta_2} \left(\xi_1 D^{\zeta_1} + \xi_5 D^{\zeta_5} \right) \left(2 - \xi_7 D^{\zeta_7} \right)}{\left(1 - \xi_7 D^{\zeta_7} - \xi_3 D^{\zeta_3} \right)^2} \tag{54}$$

Figure 11 is a plot of (54) versus $\bar{E}_b/N_0$ for a Rician parameter K = 10. Also shown are the results for the symmetric signal set obtained by setting $\phi = \pi/4$. Finally, the upper bound on the performance of uncoded QPSK in the same environment is determined from (50) with M=4.

As before, the comparable results for coherent detection are superimposed on this same figure. These results are obtained from the analysis performed in [1] and as such are given by (54) with ξ_i and ζ_i defined as follows:

$$\xi_i = e^{-K} \left[1 - \frac{1}{\sqrt{\pi}} \int_0^{\pi} \eta_i(\theta) \exp\left(\eta_i^2(\theta)\right) \operatorname{erfc} \eta_i(\theta) d\theta \right]$$

$$\eta_i(\theta) = \frac{\lambda \delta_i^2 (\bar{E}_b/N_0)}{\sqrt{1 + K}} - \sqrt{K} \cos \theta$$

$$\zeta_i = -4\lambda^2 \delta_i^2 \tag{55}$$

with δ_i^2; i = 1,2,...,7 given by (52).

Although not as obvious in Figure 7, we observe that, except for the possibility of a proportionality constant, the bit error probability performances of the differentially coherent and the coherent detection schemes

approach each other asymptotically as $\bar{E}_b/N_0$ gets sufficently large. To see this better, Figure 12 superimposes the symmetric results of Figures 7 and 11 on a single grid at the same time extending them to a broader range of $\bar{E}_b/N_0$. It is also interesting to observe from Figure 12 that the rate of decrease of P_b with $\bar{E}_b/N_0$ is much steeper for the rate 1/2 trellis coded 4DPSK (or 4PSK) case than for the rate 2/3 trellis coded 8DPSK (or 8PSK) case.

Similar observations can be made for the Rayleigh fading case (see Figures 13 and 14). In fact, here it is relatively simple to analytically demonstrate these behaviors. For symmetric rate 1/2 trellis coded 4DPSK in a Rayleigh fading environment, we have already shown that Eq. (41) is an upper bound on its bit error probability performance. Substituting (30) in (41) and letting $\bar{E}_b/N_0$ become large give the asymptotic upper bound

$$P_b \lesssim \frac{8}{(\bar{E}_b/N_0)^2} \tag{56a}$$

A similar asymptotic result for the case of coherent detection was obtained in [1] and is given by

$$P_b \lesssim \frac{9e^2}{16(\bar{E}_b/N_0)^2} \tag{56b}$$

For the symmetric rate 2/3 trellis coded 8DPSK, it is straightforward to show that both the coherent and differentially coherent bit error probabilities vary inversely with $\bar{E}_b/N_0$ [as opposed to $(\bar{E}_b/N_0)^2$].

The specific results of (56) and the statement that follows can be generalized in terms of an upper bound on P_b, for arbitrary code rate $n/(n+1)$ and the number of points in the signal constellation (i.e., M) of the form $P_b \lesssim K_0(\bar{E}_b/N_0)^{-L}$. We now investigate the interesting relationship between the exponent L and the distance structure of the error event paths in the trellis diagram.

To begin the investigation, consider the asymptotic behavior (large $\bar{E}_b/N_0$) of the pair-wise error probability for the Rayleigh channel. This can be obtained by substituting (30) in (29) and letting $\bar{E}_s/N_0$ become large with the result

$$P(\underline{x} \to \hat{\underline{x}}) \lesssim \frac{2^{\ell}}{(\bar{E}_s/N_0)^{\ell}} \prod_{n \in \eta} \frac{1}{\left| \frac{\hat{x}_n - x_n}{2} \right|^2} \tag{57}$$

where $\ell \leq N$ is the dimensionality of the set η i.e., the number of MPSK symbols in the length N sequence $\underline{x}$ for which $\hat{x}_n \neq x_n$, and $\bar{E}_s$ is related to $\bar{E}_b$ as discussed before. Now, since, from (31), the upper bound on P_b is a weighted sum of pair-wise error probabilities over all error event paths in the trellis diagram, then as $\bar{E}_b/N_0$ becomes large, the dominant term in the sum will be that corresponding to the smallest exponent of $\bar{E}_b/N_0$, i.e., the length of the shortest error event path in the trellis diagram. Thus, as mentioned above, asymptotically as $\bar{E}_b/N_0$ gets large, P_b is approximately upper bounded by $K_0(\bar{E}_b/N_0)^{-L}$ where L is determined from the shortest error event path in the trellis diagram and K_0 is determined from the product of the branch distances associated with this path, as well as the free distance of the code.

This is an interesting conclusion which has the following implications. First of all, it points out that the design of trellis coded MPSK modulations to be transmitted over the Rayleigh fading channel and differentially detected at the receiver should be guided primarily by maximizing the length of the shortest error event path (resulting in the steepest descent of P_b with $\bar{E}_b/N_0$) and the product of the branch distances on this path, with maximizing the squared free Euclidean distance as a secondary consideration. As the channel statistics tend more to a Rician channel (i.e., a strong line-of-sight component is present), the design of the code should be guided by both the length and branch distance product of the shortest error event path and the squared free Euclidean distance. Finally, as the fading disappears, resulting in an AWGN channel, the criterion for good trellis code design becomes once again only the squared free Euclidean distance as suggested by Ungerboeck [5].

An interesting side result stemming from the above is that, for trellis codes with parallel paths between states (i.e., the length of the shortest error event path is unity), the asymptotic performance of these codes on the Rayleigh channel varies inversely as $\bar{E}_b/N_0$. This result is corroborated by the numerical results in Figure 13 which correspond to the trellis diagram of Figure 9. Also, note that for the rate 1/2 trellis coded QPSK case, the shortest error event path has length two (see Figure 4). Thus, P_b varies inversely with the square of $\bar{E}_b/N_0$ as demonstrated in Figure 6 and the analytical result in Eq. (56a).

Finally, it can be shown, from the coherent detection results in [1], that the asymptotic behavior of P_b with $\bar{E}_b/N_0$ varies identically as the above, the only difference being in the proportionality constant K_0. Similar asymptotic behavior can be demonstrated for Rician channels, the

primary difference being an additional attenuation factor exp(-LK). A more complete discussion of the design and asymptotic behavior of conventional and multiple trellis codes [11] on fading channels, both for coherent and differentially coherent detection, will appear in a future report by the authors [12].

B. Ideal Channel State Information

Consider now the case where ideal channel state information is available at the receiver. This is tantamount to assuming that the receiver has absolute knowledge of the fading amplitude ρ in each symbol interval. In this case, the Gaussian decoding metric becomes

$$m(y_n, x_n) = - |y_n - 2E_s\rho_{n-1}\rho_n x_n|^2 \tag{58}$$

instead of (11). Following steps similar to (16) - (24), the conditional pair-wise error probability analogous to 25 is given by

$$P(\underline{x} \to \hat{\underline{x}}|\underline{\rho}) \leq \prod_{n\varepsilon\eta} \frac{\exp\left\{ - \dfrac{2\lambda' E_s \rho_n{}^4 |\hat{x}_n - x_n|^2 \, (1 - 4\lambda' \rho_n{}^2 N_0)}{1 - (2\lambda' \rho_n{}^2 N_0)^2 |\hat{x}_n - x_n|^2} \right\}}{1 - (2\lambda' \rho_n{}^2 N_0)^2 |\hat{x}_n - x_n|^2} \tag{59}$$

Unfortunately, even for the Rayleigh case, the average of (58) over the p.d.f. of $\underline{\rho}$ cannot be accomplished in closed form, much less the minimization over the Chernoff parameter or optimization over the signal set asymmetry. More serious than this, however, is the fact that the condition on the determinant of $I + 2\lambda' \underline{R}_n * \underline{F}_n$ given in the statement following Eq. (22) is not satisfied for

all values of ρ_n in the region $(0,\infty)$. As such, the denominator of any term on the right hand side of (58) is not always positive and thus averaging (58) over a Rayleigh or Rice distribution is not valid. In view of this, the upper bounding approach discussed thus far must be abandoned for the ideal channel state information case.

Computer simulation of the two examples in the previous section including ideal channel state information revealed that little was to be gained over the no channel state information case. The reason for this is perhaps tied to the suboptimality of the Gaussian metric since, in the case of coherent detection (where the Gaussian metric is optimum), a reasonably significant gain was achieved. Because of the above analytical difficulties and the potential lack of gain as evidenced by the computer simulations, we shall not pursue the channel state information case any further.

VI. Simulation Results

In this section, we describe and present the results of a software simulation of the system block diagram of Figure 1. The development of a simulation has a manyfold purpose. First, note that the simulation is indicative of the exact system performance whereas the theoretical bit error rate expressions are upper bounds. Second, when the number of states in the trellis diagram becomes large (e.g., 16), determining the state transition diagram and its associated transfer function is a tedious task; in such cases, simulation is the more expedient approach. Finally, system degradation due to the finite size of the interleaver/deinterleaver and decoder buffer imposed by the practical constraint on the allowable total delay is analytically intractable. Hence, to predict true system performance corresponding to the real world environment, one must again turn to simulation. In the next paragraph, we expand upon the last of these issues.

The block interleaver of Figure 1 can be regarded as a buffer with d rows which represent the depth of interleaving and s columns which represent the span of interleaving. Thus, the size of the interleaver (in symbols) is d x s. Data is written into the buffer in successive rows and read out of the buffer (the order in which it is transmitted over the channel) in columns. At the receiver, the block deinterleaver performs the reverse operation, i.e., the received soft quantized symbols are written into the buffer in successive columns and read out in rows. In practice, the interleaving depth should be chosen on the order of the maximum fade depth anticipated which, for the fading mobile satellite channel under investigation, depends on the doppler frequency or, equivalently, the vehicle speed: the smaller the doppler frequency, the longer the fade duration and vice versa. The interleaving span should be chosen on the order of the decoder buffer size. When this is done, the performance degradation (relative to that for the analytically tractable assumption of infinite interleaving depth and buffer size) will be inversely proportional to the product of interleaving size and doppler frequency.

On the other hand, the performance of the differential detector will degrade directly proportionally to doppler frequency. The reason for this is that the fading phase process varies more rapidly. Assuming infinite interleaving and decoder buffer size, one can use the same analytical approach as previously discussed to derive upper bounds on the bit error probability.

Example: Here we consider the more practical case of a rate 2/3, 16-state trellis code combined with symmetric 8PSK modulation (it was shown in [9] that, for this case, the additional coding gain produced by the addition of asymmetry to the modulation is small and thus we have chosen to ignore it.) Although, with much computational effort and the assumption of infinite interleaving and buffer size, this system can be analyzed by the approach

taken in the previous section, our interest here lies in computing the performance with limited interleaving and decoder buffer size as follows.

At the present time, this system is a candidate for NASA's Mobile Satellite Experiment (MSAT-X) project at L-band whose objective is to transmit 4800 bps of digitally encoded speech over a 5-kHz RF channel with a bit error rate of 10^{-3}. To satisfy the previously mentioned constraint on total allowable delay, the interleaving size, interleaving depth, and decoder buffer size have been optimized at this bit error rate to achieve the minimum bit signal-to-noise ratio. For the specified delay constraint (60 ms), the size of the block interleaver and deinterleaver have been chosen equal to 128 8PSK symbols (or 256 input bits). With the above chosen interleaving size, the interleaving depth has been optimized by computer simulation and found to be equal to 16 symbols. Thus, the interleaving span is 128/16 = 8 symbols over the range of doppler frequencies from 40 Hz to 200 Hz (vehicle speeds of 15 mph to 75 mph at L-band). Note, however, that for MSAT-X channels operating at low doppler frequencies such as 40 Hz, we can indeed have fade durations much longer than 16 symbols. In this case, an interleaving size of 128 symbols is not sufficient, thus a significant performance penalty can occur. Finally, with the above delay constraint imposed, the buffer size was optimized through simulation and found to be 32 symbols (or 64 bits).

Figure 15 illustrates the results of the simulation for perfect doppler tracking and time synchronization, and no intersymbol interference (ISI). In particular, Figure 15 assumes a fixed doppler frequency of 400 Hz, a fixed Rician parameter K = 10, and the two cases of no interleaving and limited interleaving as described above. Also shown are the corresponding results for no fading, i.e., $K = \infty$. From these results, it is clear that a large performance penalty is paid when interleaving is not used. Quantitatively

speaking, at a bit error rate of 10^{-3}, the performance with interleaving is 1.5 dB worse than that under ideal conditions (i.e., no fading). Without interleaving, one must pay an additional 2.5 dB in average bit energy-to-noise ratio.

References

[1] D. Divsalar and M. K. Simon, "Trellis Coded Modulation for 4800-9600 bps Transmission over a Fading Mobile Satellite Channel," JPL Publication 86-8 (MSAT-X Report 129), June 1, 1986, also to appear in the IEEE JSAC Issue on Fading Channels, February 1987.

[2] J. McGeehan and A. Bateman, "Phase-lock Transparent Tone-in-Band (TTIB): A New Spectrum Configuration Particularly Suited to the Transmission of Data over SSB Mobile Radio Networks," IEEE Trans. on Commun., Vol. COM-32, pp. 81-87, January 1984.

[3] F. Davarian, "Tone Calibration Techniques: A Digital Signaling Scheme for Mobile Applications," JPL Publication 86-40 (MSAT-X Report 138), September 15, 1986.

[4] M. K. Simon, "Dual Pilot Tone Calibration Technique (DPTCT)," IEEE Trans. on Vehic. Tech., Vol. VT-35, No. 2, May 1986, pp. 63-70.

[5] G. Ungerboeck, "Channel Coding with Multilevel/Phase Signals," IEEE Trans. on Inform. Theory, Vol. IT-28, No. 1, January 1982, pp. 55-67.

[6] M. K. Simon, J. K. Omura, R. A. Scholtz, and B. K. Levitt, Spread Spectrum Communications, Vol. 1, Computer Science Press, Rockville, MD, 1985.

[7] D. A. Johnston and S. K. Jones, "Spectrally Efficient Communication via Fading Channels using Coded Multilevel DPSK," IEEE Trans. on Comm., Vol. COM-29, No. 3, March 1981, pp. 276-284.

[8] M. Schwartz, W. R. Bennett, and S. Stein, Communication Systems and Techniques, McGraw-Hill Inc., New York, NY, 1966.

[9] M. K. Simon and D. Divsalar, "Combined Trellis Coding with Asymmetric MPSK Modulation," JPL Publication 85-24 (MSAT-X Report 109), May 1, 1985.

[10] D. Divsalar, "Performance of Mismatched receivers on Bandlimited Channels," Ph.D. Dissertation, University of California, Los Angeles, CA, 1978.

[11] D. Divsalar and M. K. Simon, "Multiple Trellis Coded Modulation (MTCM)," JPL Publication 86-44 (MSAT-X Report 141), November 15, 1986.

[12] D. Divsalar and M. K. Simon, "The Design of Trellis Codes for Fading Channels," in preparation.

Appendix A

Derivation of The Maximum-Likelihood Branch Metric for Coded MDPSK with Perfect Side Information

Referring to (5), we write w_k^* and w_{k+1} in rectangular complex notation as

$$\begin{aligned} w_k^* &\triangleq X_k^* \sqrt{2E_s}\, e^{-j\phi_k} + N_k^* = V_1 + jV_2 \\ w_{k+1} &\triangleq X_{k+1} \sqrt{2E_s}\, e^{j(\phi_k+\Delta\phi_{k+1})} + N_{k+1} = U_1 + jU_2 \end{aligned} \tag{A-1}$$

where U_1, U_2 are independent Gaussian random variables as are V_1, V_2. Furthermore U_1 and U_2 are independent of V_1 and V_2. The detector output, y_{k+1}, in the $k+1^{st}$ transmission interval is given by the product of w_k^* and w_{k+1} which, in view of (A-1), can be written as

$$\begin{aligned} y_{k+1} &\triangleq w_k^* w_{k+1} = (U_1 V_1 - U_2 V_2) + j(U_1 V_2 + U_2 V_1) \\ &\triangleq Y_1 + jY_2 \end{aligned} \tag{A-2}$$

The joint characteristic function of Y_1 and Y_2 is

$$\begin{aligned} \Phi_{Y_1,Y_2}(\omega_1,\omega_2) &= E\left\{ e^{j(\omega_1 Y_1 + \omega_2 Y_2)} \right\} \\ &= E_{\underline{V}}\left\{ E_{\underline{U}}\left\{ e^{j[(\omega_1 V_1 + \omega_2 V_2)U_1 + (\omega_2 V_1 - \omega_1 V_2)U_2]} \Big| V_1, V_2 \right\} \right\} \end{aligned} \tag{A-3a}$$

which because of the independence between U_1 and U_2 becomes

$$\begin{aligned} \Phi_{Y_1,Y_2}(\omega_1,\omega_2) = E_{\underline{V}}\Bigg\{ & E_{U_1}\left\{ e^{j(\omega_1 V_1 + \omega_2 V_2)U_1} \Big| V_1, V_2 \right\} \\ & \times E_{U_2}\left\{ e^{j(\omega_2 V_1 - \omega_1 V_2)U_2} \Big| V_1, V_2 \right\} \Bigg\} \end{aligned} \tag{A-3b}$$

Since for a Gaussian random variable X with mean $\bar{X}$ and variance σ_x^2, we have

$$\Phi_x(\omega) = E\{e^{j\omega X}\} = e^{j\bar{X}\omega - \frac{1}{2}\sigma_x^2\omega^2} \tag{A-4}$$

then applying (A-4) to each expectation in the product inside the braces of (A-3b) gives upon simplification

$$E_{U_1}\left\{e^{j(\omega_1 V_1+\omega_2 V_2)U_1}\Big|_{V_1,V_2}\right\} E_{U_2}\left\{e^{j(\omega_2 V_1-\omega_1 V_2)U_2}\Big|_{V_1,V_2}\right\}$$

$$= e^{j(\omega_1\bar{U}_1+\omega_2\bar{U}_2)V_1-\sigma^2(\omega_1^2+\omega_2^2)V_1^2/2}$$

$$\times\, e^{j(\omega_2\bar{U}_1-\omega_1\bar{U}_2)V_2-\sigma^2(\omega_1^2+\omega_2^2)V_2^2/2} \tag{A-5}$$

where σ^2 denotes the variance of U_1 and U_2 (or V_1 and V_2).

Finally, using the relation

$$E\left\{e^{j\alpha X-\sigma^2\beta X^2/2}\right\} = \frac{1}{\sqrt{1+\sigma^4\beta}} \exp\left\{\frac{2j\alpha\bar{X} - \sigma^2(\beta\bar{X}^2+\alpha^2)}{2(1+\sigma^4\beta)}\right\} \tag{A-6}$$

to evalute the expectations over V_1 and V_2 required in (A-3b), we get after much simplification

$$\Phi_{Y_1,Y_2}(\omega_1,\omega_2) = \frac{1}{1+\sigma^4(\omega_1^2+\omega_2^2)} \exp\left\{\frac{2jf_1(\omega_1,\omega_2) - \sigma^2 f_2(\omega_1,\omega_2)}{2[1+\sigma^4(\omega_1^2+\omega_2^2)]}\right\} \tag{A-7a}$$

where

$$\begin{aligned} f_1(\omega_1,\omega_2) &= (\bar{U}_1\bar{V}_1 - \bar{U}_2\bar{V}_2)\,\omega_1 + (\bar{U}_1\bar{V}_2 + \bar{U}_2\bar{V}_1)\,\omega_2 \\ f_2(\omega_1,\omega_2) &= (\omega_1^2+\omega_2^2)(\bar{U}_1^2 + \bar{U}_2^2 + \bar{V}_1^2 + \bar{V}_2^2) \end{aligned} \tag{A-7b}$$

The next step is to perform the inverse Fourier transform of (A-7a) thereby obtaining the joint probability density function of Y_1 and Y_2. In particular,

$$p_{Y_1,Y_2}(y_1,y_2) = \frac{1}{(2\pi)^2} \int_{-\infty}^{\infty} \int_{-\infty}^{\infty} \Phi_{Y_1,Y_2}(\omega_1,\omega_2)\, e^{-j(\omega_1 y_1 + \omega_2 y_2)}\, d\omega_1 d\omega_2 \qquad \text{(A-8)}$$

Making the change of variables

$$\omega_1 = R \cos \theta$$

$$\omega_2 = R \sin \theta \qquad \text{(A-9)}$$

and performing the integrations gives after some simplification

$$p_{Y_1,Y_2}(y_1,y_2) = \int_0^{\infty} W(R)\, J_0\left(\frac{R\sqrt{A^2(R) + B^2(R)}}{1 + \sigma^4 R^2}\right) dR \qquad \text{(A-10)}$$

where

$$W(R) = \frac{R}{2\pi(1 + \sigma^4 R^2)} \exp\left\{-\frac{\sigma^2 R^2(\bar{U}_1^2 + \bar{U}_2^2 + \bar{V}_1^2 + \bar{V}_2^2)}{2(1 + \sigma^4 R^2)}\right\}$$

$$A(R) = \bar{U}_1\bar{V}_1 - \bar{U}_2\bar{V}_2 - y_1(1 + \sigma^4 R^2) \qquad \text{(A-11)}$$

$$B(R) = \bar{U}_1\bar{V}_2 + \bar{U}_2\bar{V}_1 - y_2(1 + \sigma^4 R^2)$$

Finally, recognizing from (7) and (A-1) that

$$\bar{U}_1\bar{V}_1 - \bar{U}_2\bar{V}_2 = 2E_s\rho_{k+1}^2 \cos \Delta\phi_{k+1}$$

$$\bar{U}_1\bar{V}_2 + \bar{U}_2\bar{V}_1 = 2E_s\rho_{k+1}^2 \sin \Delta\phi_{k+1} \qquad \text{(A-12)}$$

$$\bar{U}_1^2 + \bar{U}_2^2 + \bar{V}_1^2 + \bar{V}_2^2 = 4E_s\rho_{k+1}^2 \quad ,$$

where we have made the assumption that ρ_k is constant over two symbol intervals, i.e., $\rho_k\rho_{k+1} = \rho_{k+1}^2$, then (A-10) together with (A-11) becomes

$$p_{Y_1,Y_2}(y_1,y_2) = \int_0^\infty \frac{R}{2\pi(1 + \sigma^4R^2)} \exp\left\{-\frac{2E_s\rho_{k+1}^2R^2\sigma^2}{(1 + \sigma^4R^2)}\right\}$$

$$\times J_0\left(R\left[\left(y_1 - \frac{2E_s\rho_{k+1}^2 \cos \Delta\phi_{k+1}}{1 + \sigma^4R^2}\right)^2\right.\right.$$

$$\left.\left. + \left(y_2 - \frac{2E_s\rho_{k+1}^2 \sin \Delta\Phi_{k+1}}{1 + \sigma^4R^2}\right)^2\right)\right] dR \qquad \text{(A-13)}$$

If we now evaluate the variance σ^2 from the noise statistics in (6), we find that $\sigma^2 = N_0$. Also recognizing from (3) that $\mathrm{Re}\{x_{k+1}\} = \cos \Delta\phi_{k+1}$ and $\mathrm{Im}\{x_{k+1}\} = \sin \Delta\phi_{k+1}$, then (A-13) can be put in the final desired form, namely,

$$p_{Y_1,Y_2}(y_1,y_2) = p(y_{k+1}|x_{k+1},z_{k+1}) = \int_0^\infty \frac{R}{2\pi(1 + N_0^2R^2)}$$

$$\times \exp\left\{-\frac{2\rho_{k+1}^2E_sN_0R^2}{1 + N_0^2R^2}\right\} \quad J_0\left(R\left|y_{k+1} - \frac{2\rho_{k+1}^2E_sx_{k+1}}{1 + N_0^2R^2}\right|\right) dR$$

(A-14)

which agrees with (13).

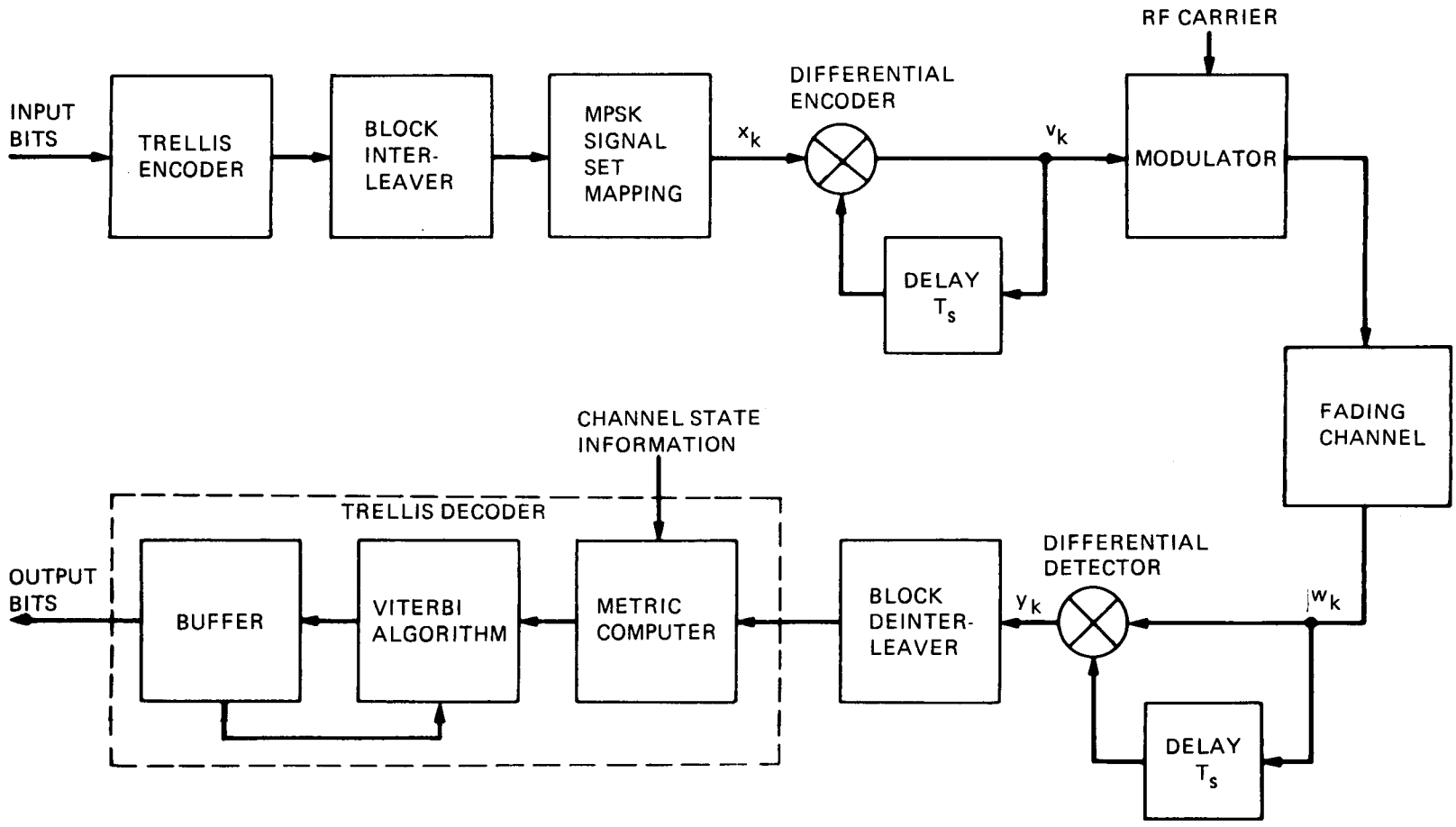

Figure 1. Block Diagram of the Trellis Coded MDPSK System

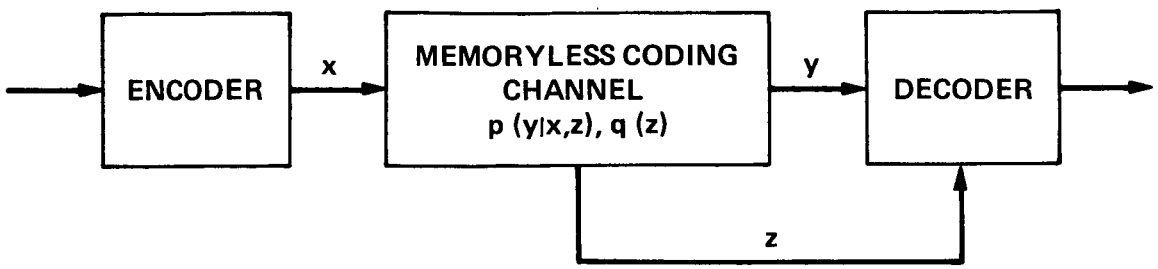

Figure 2. General Memoryless Channel

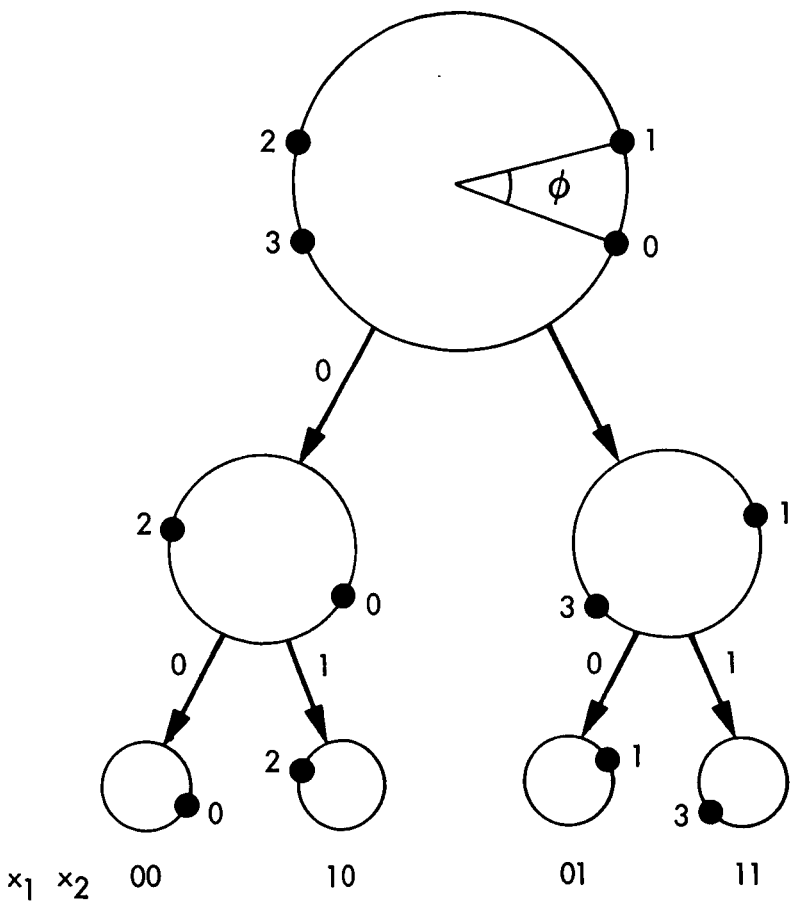

Figure 3. Set Partitioning of Asymmetric 4-PSK

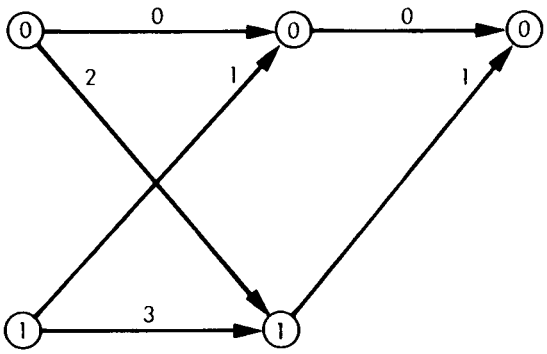

Figure 4. Trellis Diagram and MPSK Signal Assignment for 4-PSK

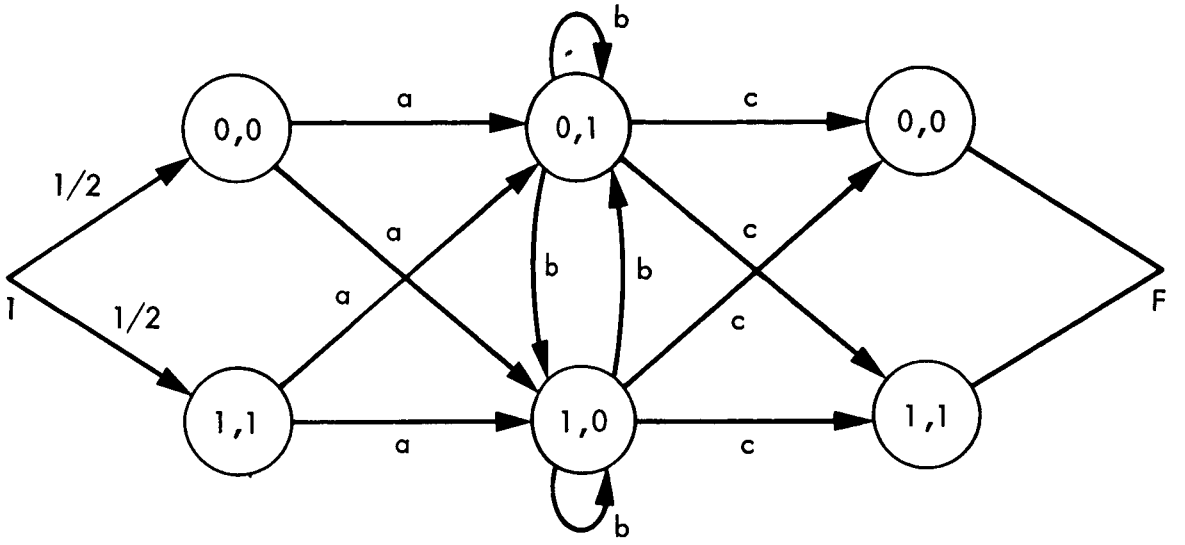

$$T(D,z) = \frac{4ac}{1-2b}$$

$$a = \frac{z}{2} D^4$$

$$b = \frac{z}{2} D^{\frac{4}{1+\alpha}}$$

$$c = \frac{1}{2} D^{\frac{4\alpha}{1+\alpha}}$$

Figure 5. Pair-State Transition Diagram for Trellis Diagram of Figure 4

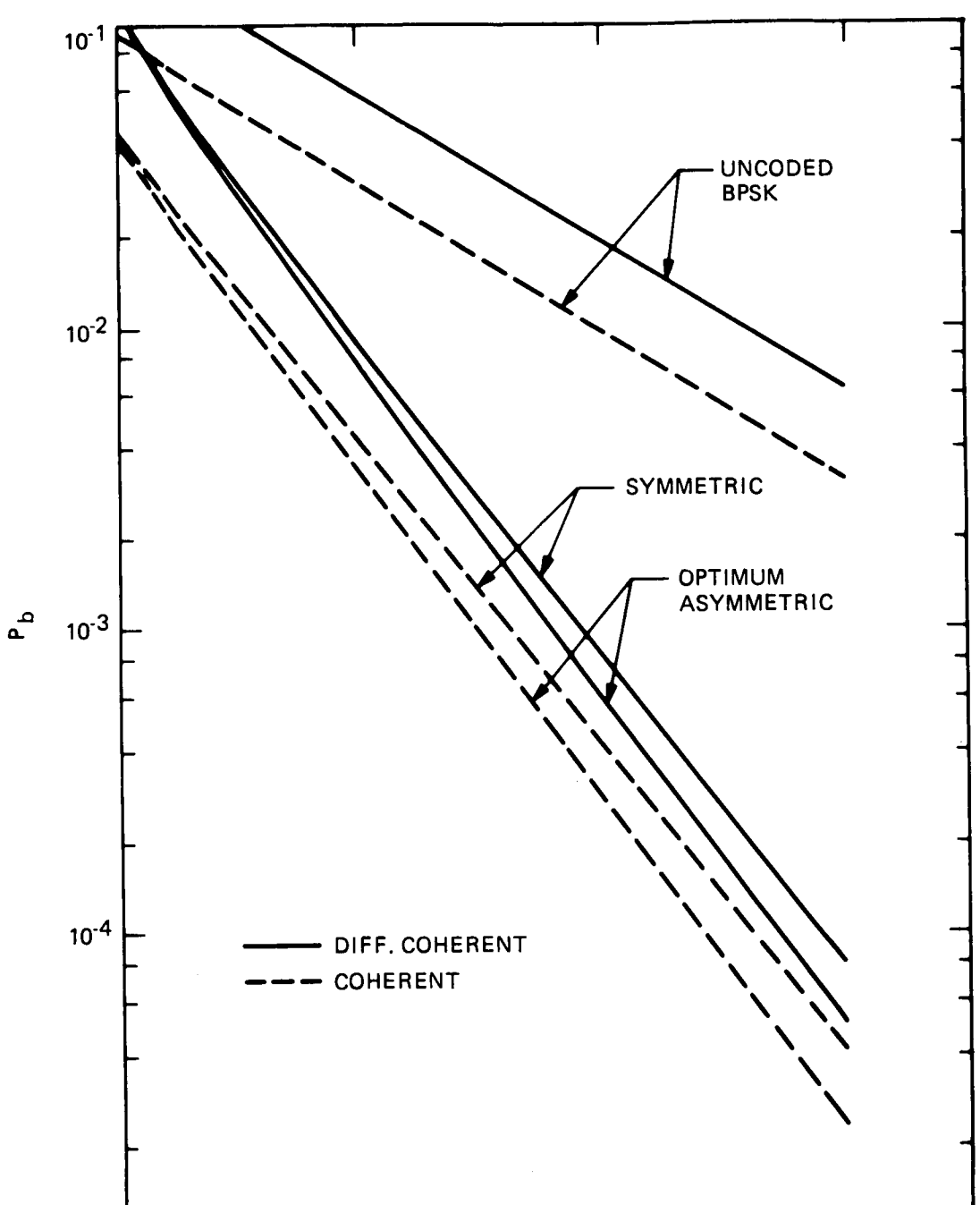

Figure 6. Bit Error Probability Performance of Rate 1/2 Trellis Coded 4-PSK in the Presence of Rayleigh Fading; 2 States, K = 0; No Channel State Information

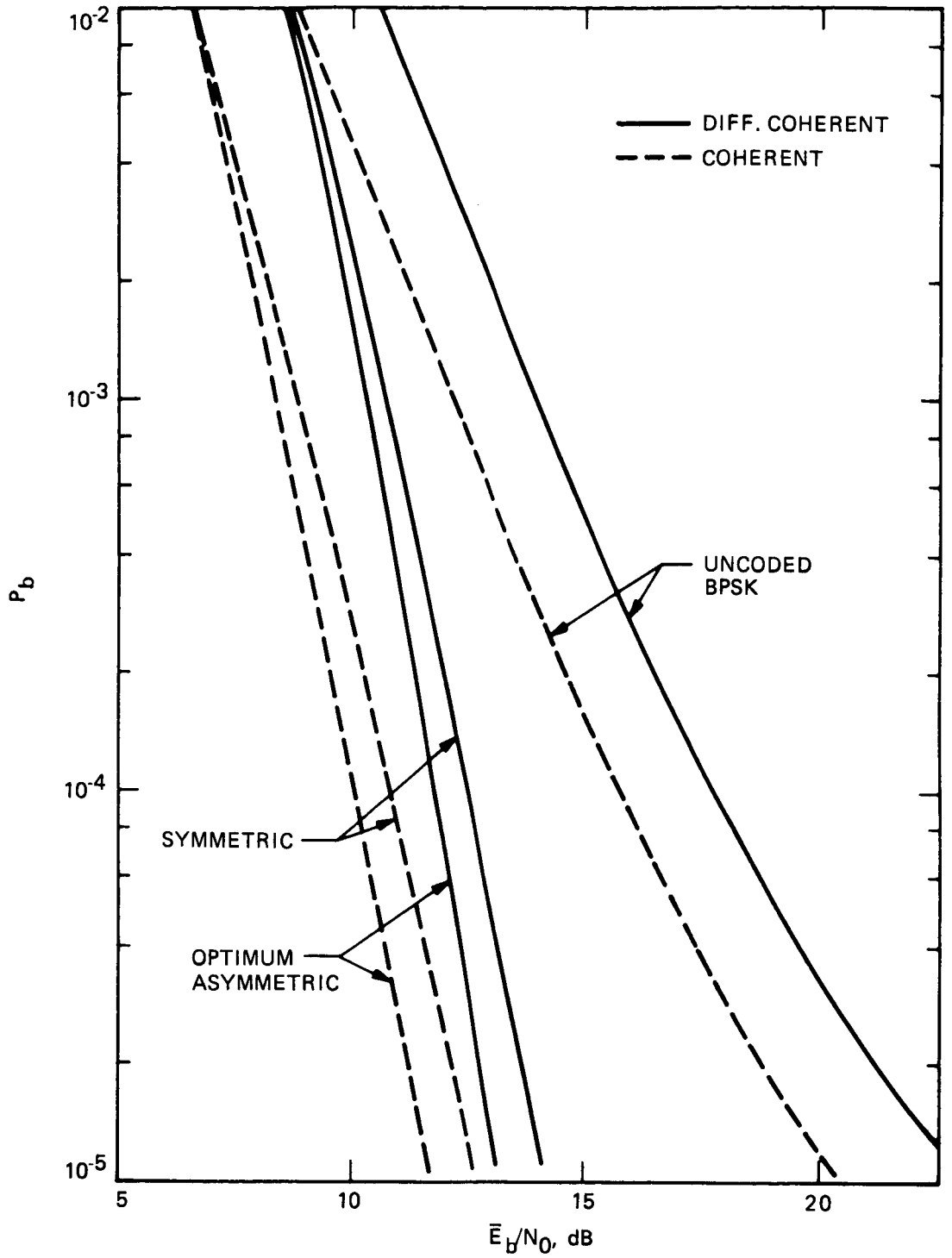

Figure 7. Bit Error Probability Performance of Rate 1/2 Trellis Coded 4-PSK in the Presence of Rician Fading; 2 States, K = 10; No Channel State Information

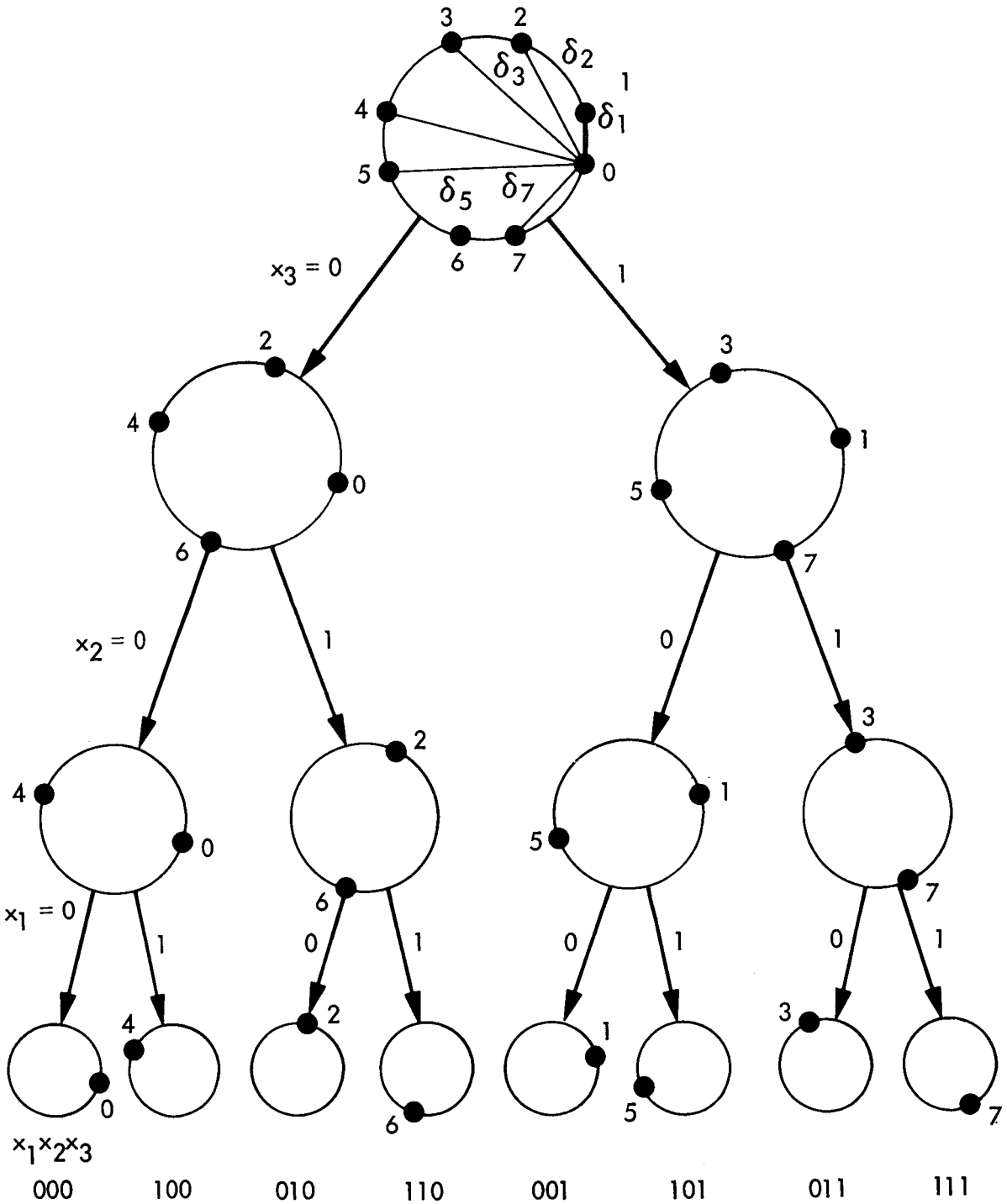

Figure 8. Set Partitioning of Asymmetric 8-PSK

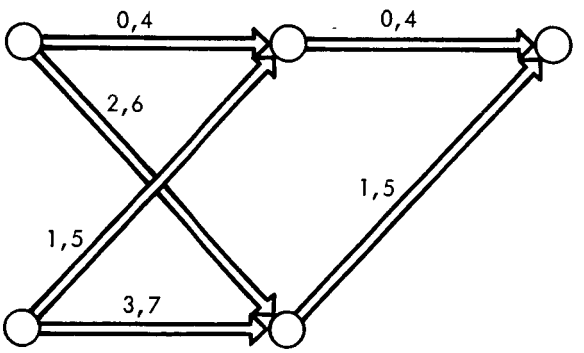

Figure 9. 2-State Trellis Diagram and Signal Assignment for 8-PSK

$$a_1 = \frac{1}{2}\left[D^{\delta_1^2} z^2 + D^{\delta_5^2} z\right]$$

$$a_2 = \frac{1}{2}\left[D^{\delta_1^2} z + D^{\delta_5^2} z^2\right]$$

$$b = \frac{1}{2}\left[D^{\delta_7^2} z + D^{\delta_3^2} z^2\right]$$

$$c = \frac{1}{2}\left[D^{\delta_6^2} (z+1)\right]$$

$$d = \frac{1}{2}\left[D^{\delta_4^2} z\right]$$

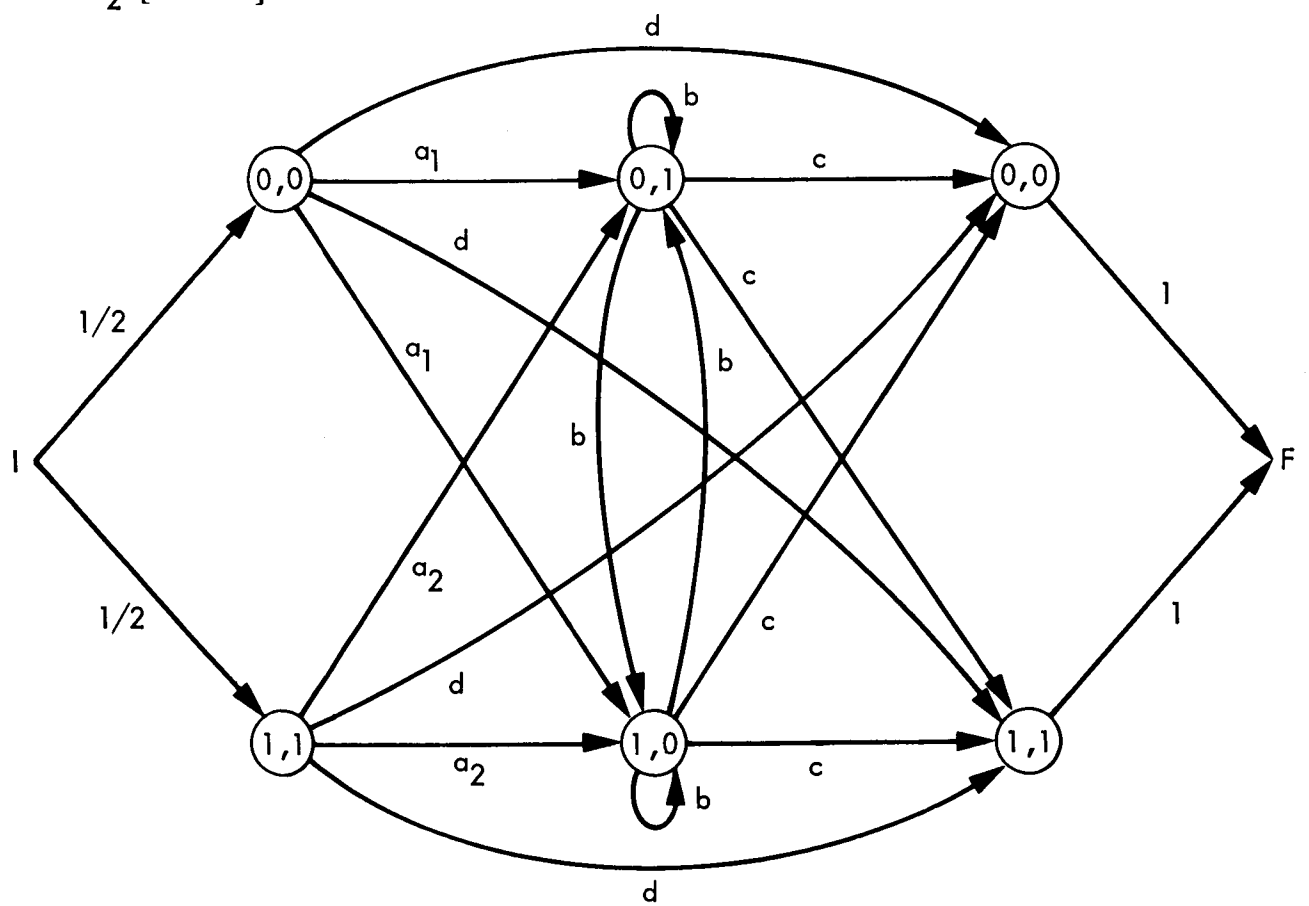

Figure 10. Pair-State Transition Diagram for Rate 2/3 Trellis Code

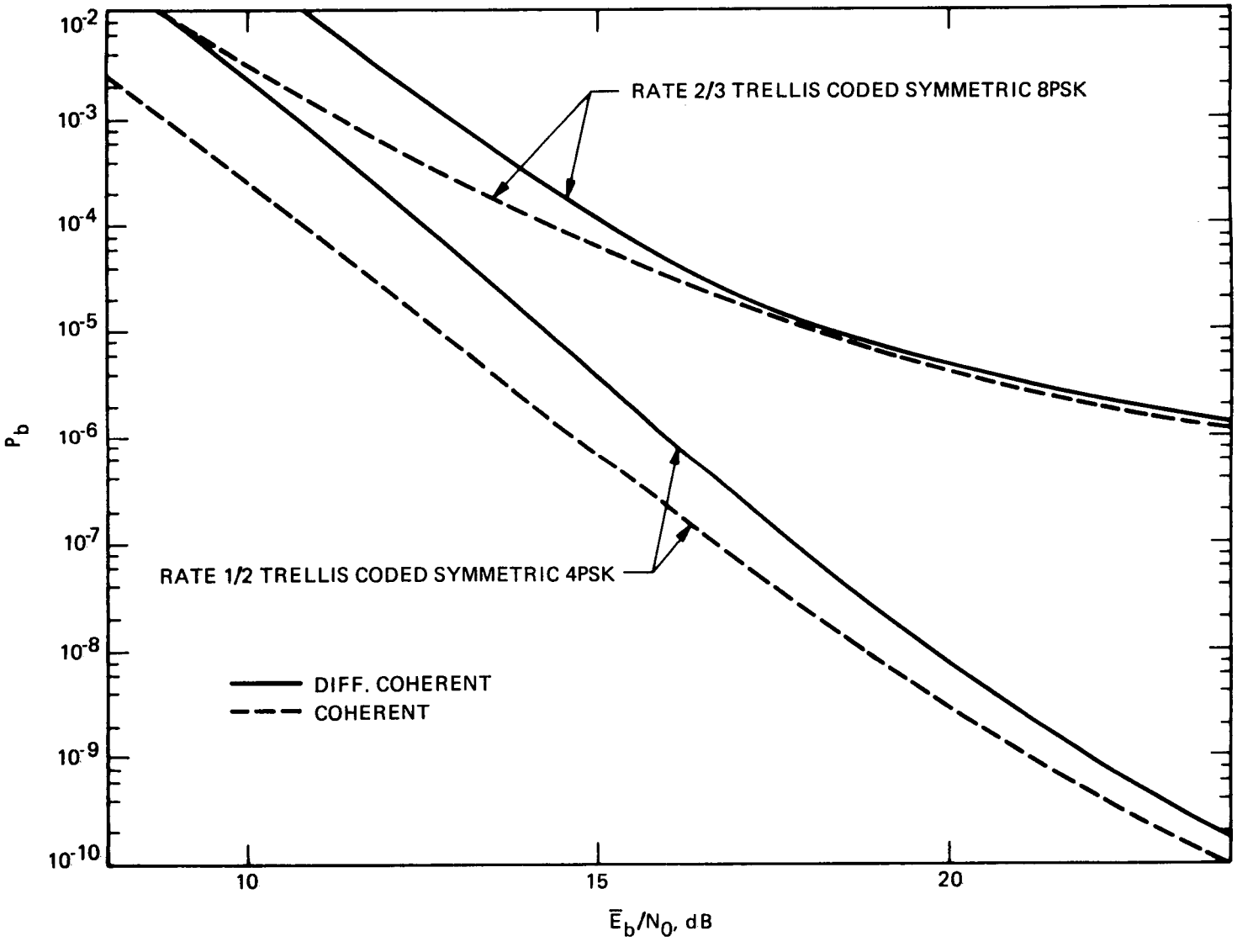

Figure 11. A Comparison of the Bit Error Probability Performances of Rate 1/2 Trellis Coded Symmetric 4-PSK and Rate 2/3 Trellis Coded Symmetric 8-PSK in Rician Fading; K = 10

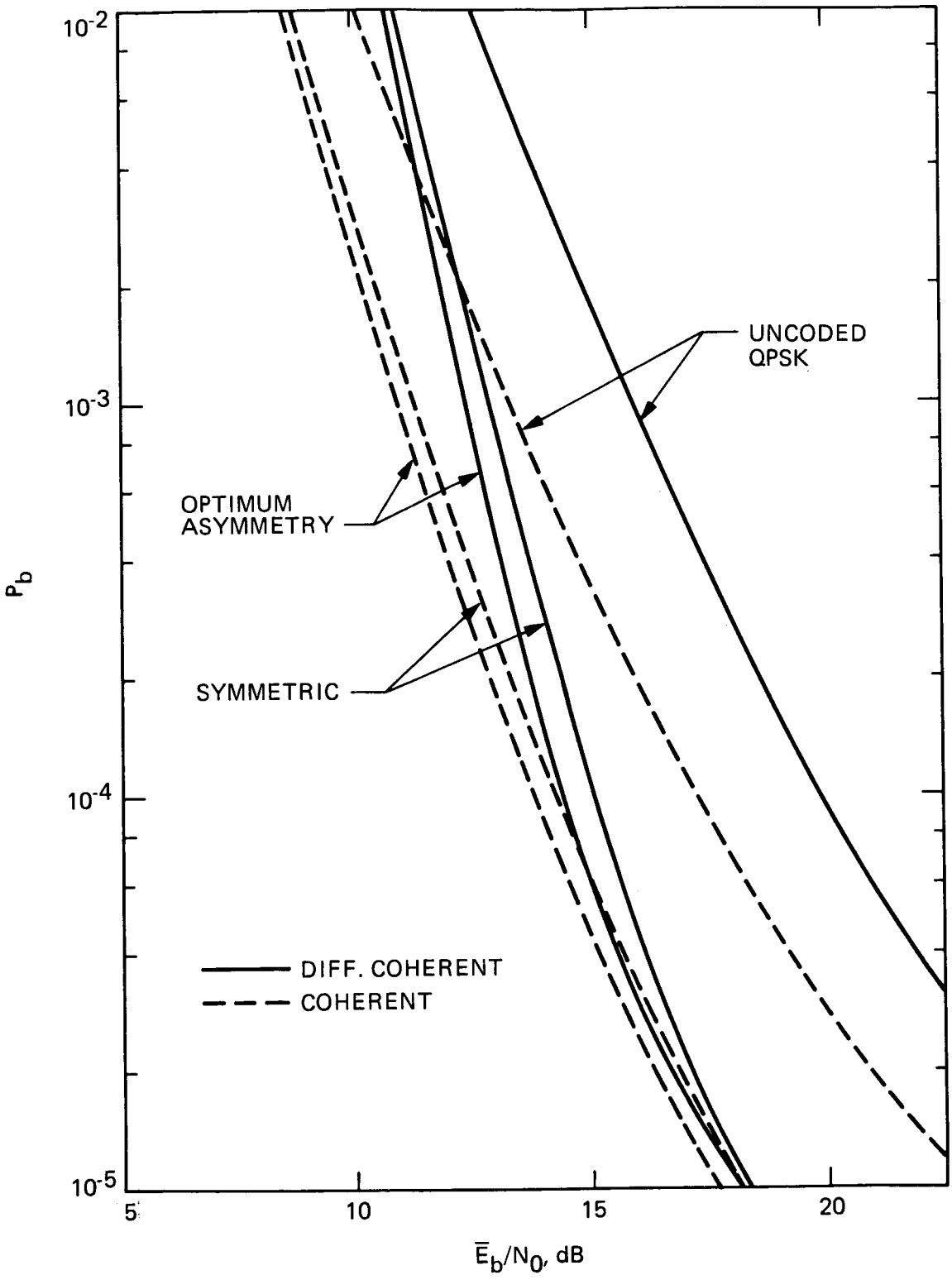

Figure 12. Bit Error Probability Performance of Rate 2/3 Trellis Coded 8-PSK in the Presence of Rician Fading; 2 State, K = 10; No Channel State Information

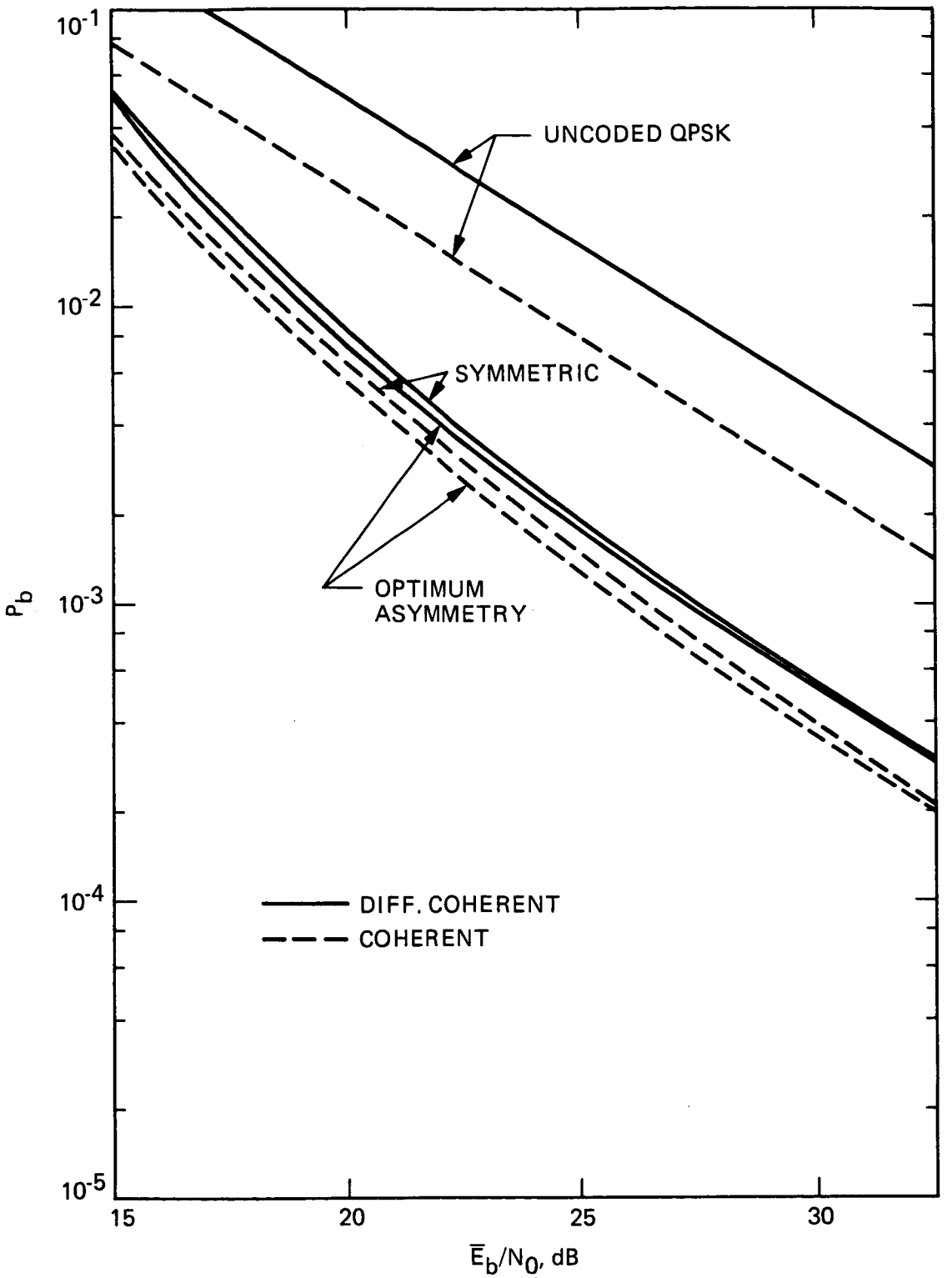

Figure 13. Bit Error Probability Performance of Rate 2/3 Trellis Coded 8-PSK in the Presence of Rayleigh Fading; 2 State, K = 10; No Channel State Information

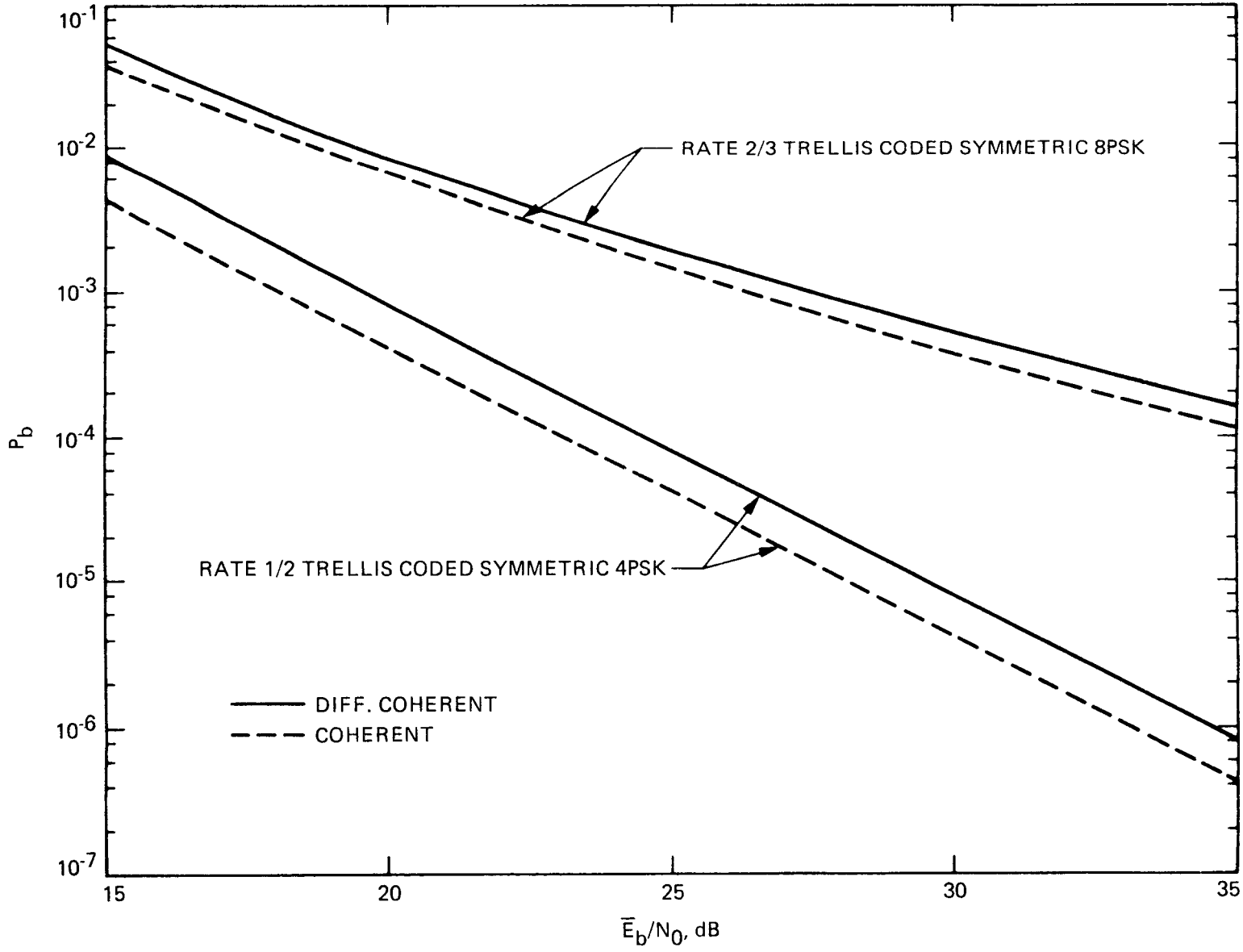

Figure 14. A Comparison of the Bit Error Probability Performances of Rate 1/2 Trellis Coded Symmetric 4-PSK and Rate 2/3 Trellis Coded Symmetric 8-PSK in Rayleigh Fading; K = 0

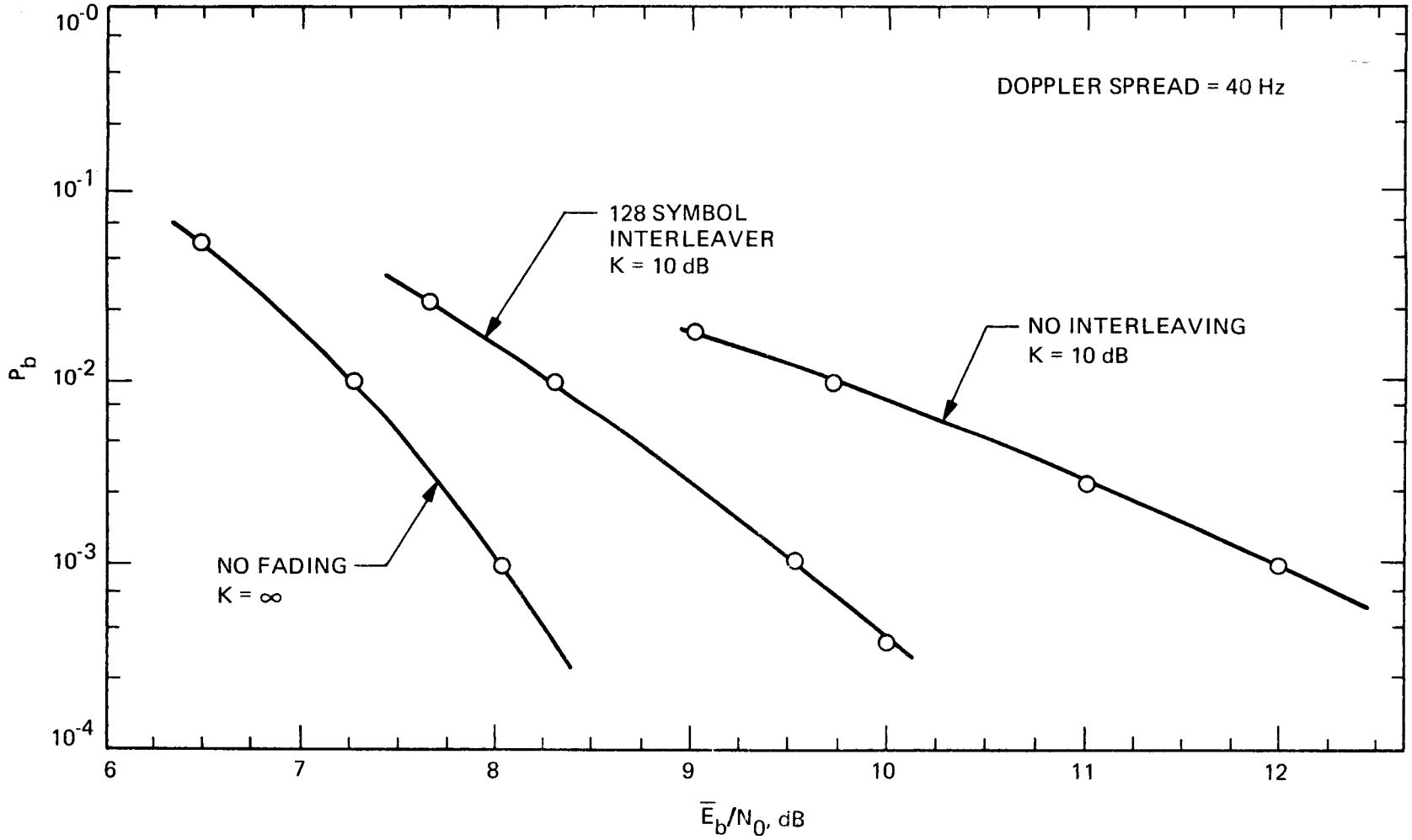

Figure 15. Simulation Results for Bit Error Rate Performance of Rate 2/3, 16 State Trellis Coded 8-DPSK